# THE TRANSPORT OF HEAT BY FLOWING GROUNDWATER IN A DISCRETE FRACTURE

by

Fan Yang

A thesis submitted to the Department of Civil Engineering

In conformity with the requirements for

the degree of Master of Applied Science

Queen's University

Kingston, Ontario, Canada

(May, 2016)

# Abstract

In typical theoretical or experimental studies of heat migration in discrete fractures, conduction and thermal dispersion are commonly neglected from the fracture heat transport equation, assuming heat conduction into the matrix is predominant. In this study analytical and numerical models are used to investigate the significance of conduction and thermal dispersion in the plane of the fracture for a point and line sources geometries. The analytical models account for advective, conductive and dispersive heat transport in both the longitudinal and transverse directions in the fracture. The heat transport in the fracture is coupled with a matrix equation in which heat is conducted in the direction perpendicular to the fracture. In the numerical model, the governing heat transport processes are the same as the analytical models; however, the matrix conduction is considered in both longitudinal and transverse directions. Firstly, we demonstrate that longitudinal conduction and dispersion are critical processes that affect heat transport in fractured rock environments, especially for small apertures (eg. 100 μm or less), high flow rate conditions (eg. velocity greater than 50 m/day) and early time (eg. less than 10 days). Secondly, transverse thermal dispersion in the fracture plane is also observed to be an important transport process leading to retardation of the migrating heat front particularly at late time (eg. after 40 days of hot water injection). Solutions which neglect dispersion in the transverse direction underestimate the locations of heat fronts at late time. Finally, this study also suggests that the geometry of the heat sources has significant effects on the heat transport in the system. For example, the effects of dispersion in the fracture are observed to decrease when the width of the heat source expands.

# Acknowledgements

Firstly, I would like to express my sincere gratitude to my thesis supervisor, Dr. Kent Novakowski, for funding this valuable study opportunity. He has always been understanding of my research issues and challenges, and has given me every opportunity to expand my knowledge. As the head of the department, his leadership is well recognized by the students and colleagues. His professional skills in hydrogeology and management will guide me through the rest of my career.

Secondly, I would like to thank the individuals who had influenced me throughout the past two and a half years. Dr. Bernard Kueper, thank you for teaching me about contaminants transport and remediation. Dr. Kevin Mumford, thank you for walking me through my first conference presentation. I would also like to thank Dr. Robert Walsh for his supervision during my internship at Geofirma Engineering. Special thanks to Dr. Brent Sleep, Dr. Glaucia Lima and the Natural Science and Engineering Research Council (NSERC) for providing the Remediation Education Network (RENEW). My academic knowledge and soft skills are greatly benefited from the workshops and webinars that were offered by the RENEW program. Additionally, the support of Maxine Wilson and Debbie Ritchie is greatly appreciated.

Finally, I would like to thank my friends who had supported me selflessly, especially Andrew Logan, Diana Zhang, Eric Martin, Issam Bou Jaoude, Kurt Wood, Omar Khader and Sean Bryck.

# Table of Contents

Abstract……..ii
Acknowledgements……...iii
List of Tables……....v
List of Figures……viii
Chapter 1 Introduction ..... 1
1.2 Literature Cited ..... 5
Chapter 2 The Transport of Heat by Flowing Groundwater in A Discrete Fracture..... 6
2.1 Introduction..... 6
2.2 Theory ..... 10
2.2.1 Analytical Model..... 11
2.2.2 Analytical Solutions ..... 16
2.2.3 Numerical Model ..... 21
2.3 Method ..... 25
2.3.1 Input Parameters ..... 26
2.3.2 Heat Front and Error ..... 28
2.4 Results and Discussion ..... 31
2.4.1 Effects of Matrix Conduction ..... 31
2.4.2 Significance of Longitudinal Conduction in the Fracture ..... 33
2.4.3 Significance of Longitudinal Dispersion in the Fracture ..... 36
2.5 Conclusions..... 48
2.6 Literature Cited ..... 50
Chapter 3 Conclusions and Recommendations..... 54
Appendix A 2-D Analytical Solution Development ..... 57
Appendix B Numerical Model Verification..... 61
Appendix C Sample HydroGeoSphere Input Code ..... 65
Appendix D Sample Matlab Code for Analytical Solutions..... 70
Appendix D Governing Equations for Heat Transport from the HydroGeoSphere User Manual ..... 75

# List of Figures

Figure 1.1: (a) Two-dimensional fracture-matrix system. The matrix extends to infinity in both x and z directions. (b) Plan view of the fracture in the y-z plane, the system is confined with no flux boundaries in the y direction. ..... 15
Figure 2: Grid for the two-dimensional numerical model with a discrete fracture. For the large aperture case, the model dimension is set to 30 m by 30 m. For the small aperture case, the dimension is set to 16 m by 10 m in the x-and z-directions, respectively. The grid is shown for illustration. The actual grid is much finer (starting from 0.001 m in the vicinity of the fracture and gradually increasing to 0.1 m in the x-direction)..... 24
Figure 3: Temperature along the fracture at 5 days given by the 1-D general solution (red) and the 1-D conductive solution (blue), at aperture= 500 μm, flow velocity= 5 m/day and an injection temperature of 1 °C. ..... 30
Figure 4: Comparison between the conductive solution (red) versus the numerical solution (blue) for a 1 °C temperature contour in the domain, aperture, 2b =1000 μm, flow velocity, v = 50 m/day and injection temperature 15 °C. ..... 33
Figure 5: Error in heat front position due to neglecting longitudinal thermal conduction in 1-D heat transport in a fracture. (a) Small Aperture 2b=100 μm, (b) Large Aperture 2b=1000 μm. ..... 35
Figure 6: Error in heat front position due to neglecting dispersion in 1-D heat transport in a fracture. (a) Large Aperture 2b=1000, (b) Small Aperture 2b=100. Thermal dispersivity ($\alpha$) equals to 0.1 m. ..... 37
Figure 7: The 0.01 °C temperature contour obtained from the 2-D dispersive solution, equation [18], and the 2-D conductive solution, equation [20], in the plane of the fracture. The flow velocity equals 40 m/day, and fracture aperture equals 1000 μm. ..... 39
Figure 8: Error in the heat front position due to neglecting thermal dispersion in 2-D heat transport in the plane of the fracture. Longitudinal dispersivity $\alpha_z$= 0.1 m, transverse dispersivity $\alpha_y$= 0.01 m, $2b$= 1000 μm, and $v$= 40m/day. ..... 40
Figure 9: Error in the heat front position due to neglecting thermal dispersion in 2-D heat transport in the plane of the fracture. Longitudinal dispersivity $\alpha_z$= 0.1 m, transverse dispersivity $\alpha_y$= 0.01 m, $2b$=100 μm, and $v$=1 m/day. ..... 41
Figure 10: The 1 °C temperature contour at 250 days obtained from the numerical model (HGS). The fracture is oriented vertically and is located x=15 m. Heat conduction is two-dimensional in the matrix. The red line and the black line represent simulations that were conducted with and without dispersion,

respectively. The flow velocity equals 50 m/day, fracture aperture equals 1000 μm, and thermal dispersivity equals 1.0 m..... 43
Figure 11: The 1 °C temperature contour at 200 days obtained from the numerical model (HGS). The fracture is oriented vertically and is located x=8 m. Heat conduction is two-dimensional in the matrix. The red line and the black line represent simulations that were conducted with and without dispersion, respectively. The flow velocity equals 10 m/day, fracture aperture equals 100 μm, and thermal dispersivity equals 1.0 m..... 44
Figure 12: Error of the heat front position due to neglecting thermal dispersion in the fracture using the numerical model (HGS). At a flow velocity of 50 m/day, an aperture of 1000 μm and thermal dispersivity ($\alpha$) of 1.0 m. ..... 45
Figure 13: Error of the heat front position due to neglecting thermal dispersion in the fracture using the numerical model (HGS), at a flow velocity of 10 m/day, an aperture of 100 μm and thermal dispersivity ($\alpha$) of 1.0 m. ..... 46
Figure 14: Comparison between the 1-D analytical solution and the numerical solution where the thermal dispersion is neglected for both solution methods. The error is calculated at a flow velocity of 10 m/day and an aperture of 100 μm, where the true heat front is calculated in the presence of thermal dispersivity The value of thermal dispersivity ($\alpha$) equals to 0.1 m in the general solution, and it equals to 1.0 m in the numerical solution for the true heat front. The discrepancies between the results are mainly due to longitudinal conduction in the matrix. ..... 48

Figure A. 1 Comparison between the temperature breakthrough results from the analytical solution and HGS. At aperture, 2b= 300 um, and flow velocity 0.05 m/s, the two solutions show strong agreement (note that the two curves overlap each other). This indicates the effects of longitudinal matrix conduction are insignificant at the extreme flow condition..... 61
Figure A. 2 Comparison between the temperature breakthrough results from the analytical solution and HGS. At aperture, 2b= 300 um, and flow velocity 0.0005 m/s, temperature differences are observed between the analytical solution and HGS due to the inclusion of 2-D conduction in the matrix in the numerical model..... 62
Figure A. 3 The mesh in the numerical model is refined to study the effects of discretization. At a finer mesh, discrepancies between the analytical and numerical models are still observed. This indicates the differences between the two solutions are not influenced by the discretization. ..... 63
Figure A. 4 Comparison between longitudinal conduction in the fracture (red) versus pure advection (blue) for a 0.01 °C temperature contour in the domain, aperture, 2b =200 μm and flow velocity, v = 2 m/day. The heat penetration in the matrix is one magnitude deeper than the fracture. This suggests that the

analytical solutions underestimate the temperature in the fracture. The underestimation of the heat front in the fracture is due to the simplification made in the matrix equation which restricts conduction in the horizontal direction. ..... 64

# List of Tables

Table 1: Thermal transport properties and initial conditions ..... 27

# Chapter 1

# Introduction

The concept of heat transport in fractured rock is a fundamental component in the understanding and analysis of aquifer thermal energy storage (e.g. Bödvarsson and Tsang, 1982; Li, 2014). Prediction of the temperature field resulting from the thermal transport in a fracture relies on both analytical and numerical modeling (e.g. Bödvarsson and Tsang 1982; Doe et al. 2014). Modeling of thermal plume migration can be difficult due to the heterogeneity of the fracture networks in the field. In the typical analytical approach, a fracture network can be simplified to either a single discrete fracture model or a series of equally spaced parallel fractures model as shown in Figure 1.1 (a) and Figure 1.1 (b), respectively (Bödvarsson and Tsang, 1982; Yang et al., 1998). The differences between the two models are the boundary conditions in the *x*-direction. For example, the matrix extends from positive to negative infinity in the *x*-direction in the single fracture model whereas it is confined with no heat flow boundaries (adiabatic) in the parallel fractures model. Although different boundary conditions are applied, the governing heat transport processes in the fracture and the matrix are the same.

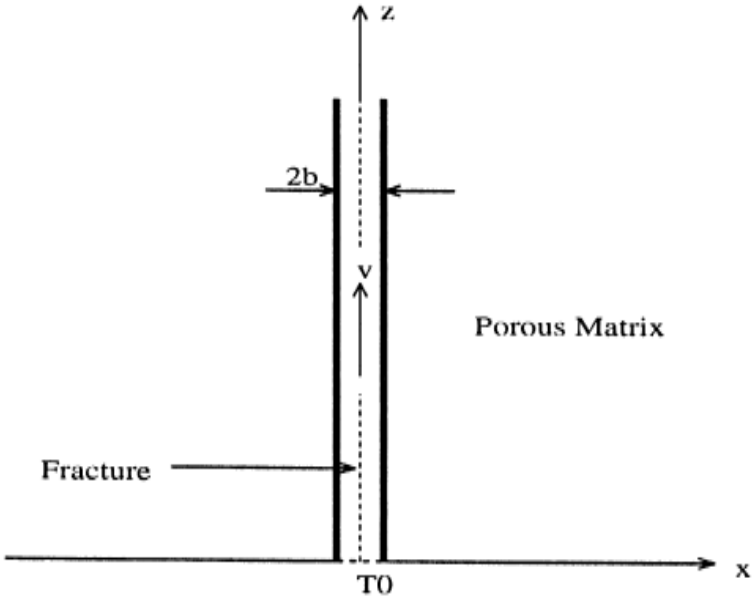


(a)

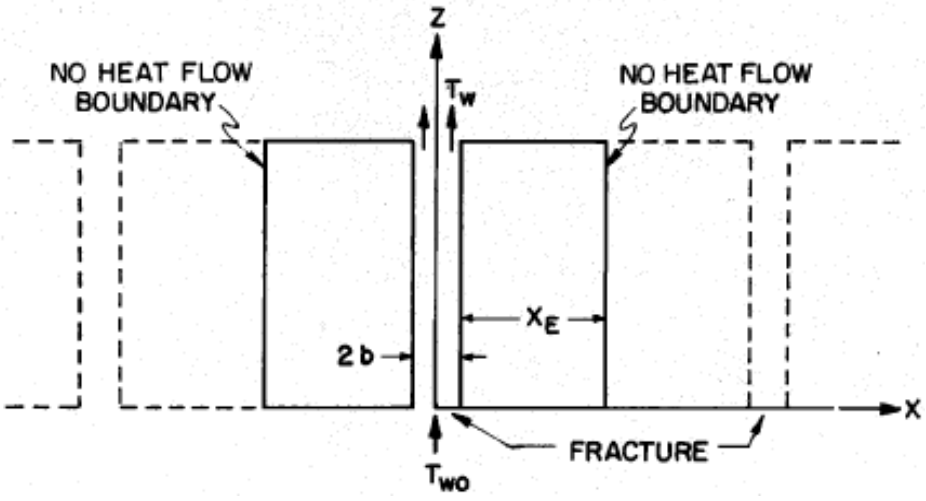


(b)

**Figure 1.1: Typical analytical fracture-matrix model. (a) A single infinitely extended discrete fractured model. The confining matrix is impermeable and extends infinity in the lateral direction (Yang et al., 1998). (b) An infinite series of parallel fractures model (Bödvarsson and Tsang, 1982). The fracture spacing and fracture aperture are constant.**

A fracture with substantial permeability provides preferential pathways for fluid flow (Oron and Berkowitz, 1998; Neuman, 2005; Novakowski et al., 2006). Groundwater flows in the fracture and results in advective transport of heat. In addition, the heterogeneity of the fluid velocity which occurs in the fracture plane will result in the dispersive transport of heat. This dispersion mechanism is well documented in the solute transport literatures and is influenced by the velocity distribution across the fracture aperture, roughness of the fracture surfaces, variation of the fracture apertures and preferential flow paths (Novakowski et al., 1985; Gelhar et al., 1992; Bodin et al., 2003; Zhou et al., 2007). Other than advective and dispersive transport, conductive transport in the flow direction is also considered as an important process that affects heat transport in the fracture (Yang et al., 1998; Li, 2014). In addition, as hot fluid flows in the fracture, it releases energy to the confining matrix where groundwater flow is absent. Heat transport in the porous matrix is governed by conduction, and the transport efficiency is dependent on heat capacity and density of the matrix, as well as the temperature gradient between across the fracture-matrix interface (Özisik, 1980). Transport is conduction dominated for thermal Peclet number less than one (Rau et al., 2012). Free convection in the porous matrix is often neglected due to the slow velocity comparing to the velocity in the fracture (Li, 2014).

The single fracture and the parallel fracture models have been presented in many forms to serve the needs of different geothermal applications (e.g. Gan and Elsworth, 2014; Wu et al., 2015). In these models, longitudinal dispersion and conduction have been commonly neglected, assuming that advective transport via groundwater flow and heat conduction

into the matrix are the dominant processes. The error introduced by this simplification has rarely been discussed in the past and more recent literature articles. Studies conducted in porous media however suggest conduction and dispersion have significant impacts on the distribution of the thermal plume (Metzger et al., 2004; Saar, 2011; Rau et al., 2012). Based on these studies, analytical models which neglect dispersion and conduction can significantly underestimate the distribution of the temperature profile and movement of the heat front. In addition, recent studies suggest conduction in the matrix should be considered as a two-dimensional process. Models which neglect longitudinal conduction in the matrix are shown to significantly overestimate the fracture temperature (Li, 2014; Ruiz Martínez et al., 2014). Therefore, the effects of dispersion and conduction need to be explored, with considering matrix conduction in both longitudinal and transverse directions under a range of flow conditions.

This thesis explores the effects of longitudinal conduction and dispersion in the fracture heat transport equation for large and small aperture cases. We assume thermal dispersivity is comparable to solute dispersivity and occurs through approximately the same physical processes (for example, due to aperture heterogeneity, closure, and fracture wall roughness). In Chapter 2, analytical and numerical solutions were used to estimate the percentage errors that resulted when longitudinal conduction and dispersion were neglected. Two source geometries were considered, one in which the source is located as a discrete point or plane in the fracture and the second in which the source is distributed across the fracture origin and the surrounding matrix. Chapter 3 summarizes the results and findings of this study.

## 1.2 Literature Cited


Bodin, J., Delay, F., de Marsily, G., 2003. Solute transport in a single fracture with negligible matrix permeability: 1. fundamental mechanisms. Hydrogeology Journal 11, 418–433.

Bödvarsson, G.S., Tsang, C.F., 1982. Injection and Thermal Breakthrough in Fractured Geothermal Reservoirs. Journal of Geophysical Research 87, 1031–1048.

Doe, T., Mclaren, R., Dershowitz, W., 2014. Discrete Fracture Network Simulations of Enhanced Geothermal Systems, in: 39th Workshop on Geothermal Reservoir Engineering. Stanford.

Gan, Q., Elsworth, D., 2014. Thermal drawdown and late-stage seismic-slip fault reactivation in enhanced geothermal reservoirs. Journal of Geophysical Research 1–14.

Gelhar, L.W., Welty, C., Rehfeldt, K.R., 1992. A critical review of data on field-scale dispersion in aquifers. Water Resources Research 28, 1955–1974.

Li, W., 2014. Numerical and Analytical Modeling of Heat Transfer between Fluid and Fractured Rocks. Massachusetts Institute of Technology.

Metzger, T., Didierjean, S., Maillet, D., 2004. Optimal experimental estimation of thermal dispersion coefficients in porous media. International Journal of Heat and Mass Transfer 47, 3341–3353.

Neuman, S.P., 2005. Trends, prospects and challenges in quantifying flow and transport through fractured rocks. Hydrogeology Journal 13, 124–147.

Novakowski, K., Bickerton, G., Lapcevic, P., Voralek, J., Ross, N., 2006. Measurements of groundwater velocity in discrete rock fractures. Journal of Contaminant Hydrology 82, 44–60.

Novakowski, K., Evans, G., Lever, D., Raven, K., 1985. A field example of measuring hydrodynamic dispersion in a single fracture. Water Resources Research 21, 1165–1174.

Oron, A.P., Berkowitz, B., 1998. Flow in rock fractures: The local cubic law assumption reexamined. Water Resources Research 34, 2811.

Özisik, M.N., 1980. Heat Conduction. John Wiley & Sons, 605 Third Avenue, New York.

Rau, G.C., Andersen, M.S., Acworth, I.R., 2012. Experimental investigation of the thermal dispersivity term and its significance in the heat transport equation for flow in sediments. Water Resources Research 48.

Ruiz Martínez, Á., Roubinet, D., Tartakovsky, D.M., 2014. Analytical models of heat conduction in fractured rocks. Journal of Geophysical Research 119, 83–98.

Saar, M.O., 2011. Review: Geothermal heat as a tracer of large-scale groundwater flow and as a means to determine permeability fields. Hydrogeology Journal 19, 31–52.

Wu, B., Zhang, X., Jeffrey, R.G., Bunger, A.P., Huddlestone-Holmes, C., 2015. Perturbation analysis for predicting the temperatures of water flowing through multiple parallel fractures in a rock mass. International Journal of Rock Mechanics and Mining Sciences 76, 162–173.

Yang, J., Latychev, K., Edwards, R.N., 1998. Numerical computation of hydrothermal fluid circulation in fractured Earth structures. Geophysical Journal International 135, 627–649.

Zhou, Q., Liu, H.H., Molz, F.J., Zhang, Y., Bodvarsson, G.S., 2007. Field-scale effective matrix diffusion coefficient for fractured rock: results from literature survey. Journal of Contaminant Hydrology 73, 161–187.

# Chapter 2

## THE TRANSPORT OF HEAT BY FLOWING GROUNDWATER IN A DISCRETE FRACTURE

### 2.1 Introduction

Heat transport via groundwater migration in fractured rocks is a fundamental component of the performance of geothermal systems and the application of thermal remediation methods for groundwater contamination (Bödvarsson and Tsang, 1982; Ferguson, 2007; Baston and Kueper, 2009). Our understanding of heat transport in these settings is however limited due to the heterogeneity of the fracture network in which the hydraulic conductivity and the fracture connectivity could vary by several orders of magnitude within the same site (Berkowitz, 2002). In recent years, several analytical and numerical solutions have been developed to investigate the advancement of a heat front and the evolution of a temperature distribution during fluid injection into a single discrete fracture. In these discrete fracture models, heat transport through the fracture and through the host rock are often considered separately using two coupled differential equations (e.g. Bödvarsson and Tsang, 1982; Sauty et al., 1982b; Yang et al., 1998; Cheng et al., 2001; Baston and Kueper, 2009; Ruiz Martínez et al., 2014)

In the rock matrix where fluid velocity is negligible, thermal conduction is the dominant transport process (Rau et al., 2012). For example, earth materials with permeabilities below $5 \times 10^{-17}$ $m^2$ result in heat-conduction-dominated systems (Saar, 2011). Thus, heat transport in low permeability host rocks like dolostone, limestone, and granite are

dominated by thermal conduction in the absence of fractures (Zhou et al., 2007; Ruiz Martínez et al., 2014; Guo, 2015).

For heat transport in a fracture, in addition to thermal conduction, heat is also transported through advection and dispersion via groundwater flow. A fracture with substantial permeability provides preferential paths for fluid flow (Oron and Berkowitz, 1998; Neuman, 2005; Novakowski et al., 2006). In addition, the heterogeneity of the fluid velocity which occurs in the fracture plane will result in the spatial spreading of the heat plume. This dispersion mechanism is well documented in the literature for solute transport, and it is influenced by the velocity distribution across the fracture aperture, roughness of the fracture surfaces, variation of the fracture apertures, and preferential flow paths (Novakowski et al., 1985; Gelhar et al., 1992; Bodin et al., 2003; Zhou et al., 2007).

Although dispersion and conduction are critical processes that may impact heat transfer in fractures, very few studies have included these two processes together when simulating heat transport in fractured rocks (e.g. Yoshida et al., 2002; Ferguson, 2007; Bagalkot and Kumar, 2014; Li, 2014). Studies conducted in porous media however suggest conduction and dispersion have significant impacts on the distribution of the thermal plume (e.g. Metzger et al., 2004; Saar, 2011; Rau et al., 2012). Ganguly and Kumar (2014) developed analytical solutions to model the temperature distribution in a confined geothermal aquifer five meter in thickness. This study shows that at injection rate of 0.3 $m^3/s$, the advancement of a temperature front is almost three times faster when longitudinal

conductive and dispersive transport in the geothermal aquifer are considered. In a study conducted by Molina-Giraldo et al. (2011) using analytical models, it was concluded that thermal dispersion has a large effect on the temperature plume distribution in highly permeable and homogeneous media (with Darcy velocities higher than $10^{-8}$ m/s). In field experiments conducted by Sauty et al. (1982) over travel distance of 13 m, longitudinal thermal dispersivity is estimated to be one meter for a range of injection rate between $7.0 \times 10^{-4}$ $m^3/s$ (2.5 $m^3/h$) and $2.0 \times 10^{-3}$ $m^3/s$ (7 $m^3/h$). It is also observed that thermal dispersivity was of the same order of magnitude as solute dispersivity obtained at the same site. This suggests thermal dispersion is as important as solute dispersion in porous media settings.

Longitudinal conduction and dispersion are often neglected from the fracture heat transport equation assuming advective transport via groundwater flow is predominant (e.g. Bödvarsson and Tsang, 1982; Lu and Xiang, 2012; Gan and Elsworth, 2014; Wu et al., 2015). There are only a few studies which discuss the error introduced by neglecting longitudinal conduction and dispersion (e.g. Cheng et al., 2001; Jung and Pruess, 2012; Li, 2014). In the numerical simulation conducted by Jung and Pruess (2012), neglecting conduction is shown to have minor effects on the temperature distribution. The simulation, however, was performed using a 50 m long single discrete fracture with an aperture of 20000 μm (2 cm) and flow velocity of $4.0 \times 10^{-4}$ m/s (35 m/day). Similarly, substituting the conductivity of water into the classical Taylor dispersion equation, Cheng et al. (2001) suggests eliminating longitudinal conduction and dispersion yields less than five percent error after 10 days of heat injection in a 1000 m long discrete

fracture. The study was performed in a similarly large fracture with aperture 20000 μm (2 cm) and flow velocity of 1.0 x $10^{-2}$ m/s (864 m/day). The conclusion drawn from Cheng et al. (2001) is referenced by many studies which neglect longitudinal conduction and dispersion in the heat transport equations for the fracture (e.g. Yang and Yeh, 2009; Ghassemi and Zhou, 2011; Zeng et al., 2013; Wu et al., 2015). It is important to note that the flow conditions and fracture apertures that were considered in these studies range much more widely than what was considered in Cheng et al. (2001) and Jung and Pruess (2012). Specifically, the fracture aperture ranged widely between 50 μm and 5x$10^5$ μm, and the flow velocities varied from 0.007 $m^3$/s to 0.1 $m^3$/s in these studies. However, as reviewed above dispersion is a function of flow velocity and travel distance, therefore the conclusions drawn from Cheng et al. (2001) and Jung and Pruess (2012) may not be valid at all aperture and flow conditions. In addition, Taylor dispersion only describes local mixing across the fracture aperture but ignores field-scale mixing which could be orders of magnitude larger (Novakowski et al., 1985; Zhou et al., 2007).

Other than the insufficient consideration of flow conditions, the conclusions from Cheng et al. (2001) are also limited by the assumption made in the matrix equation where heat is restricted to conduction in the direction perpendicular (in the transverse direction) to the fracture. Recent studies suggest conduction in the matrix should be considered as a two-dimensional process. Models which neglect longitudinal conduction in the matrix are shown to significantly overestimate the heat transport in the fracture (Li, 2014; Ruiz Martínez et al., 2014). Therefore, the effects of dispersion and conduction in the fracture

require reevaluation in consideration of matrix conduction in both longitudinal and transverse directions under a range of flow conditions.

The objective of this study is to investigate the effects of longitudinal conduction and dispersion on heat transport in a discrete fracture embedded in a rock matrix of low permeability. This is conducted for two source conditions, one in which the source is located as a discrete point or plane in the fracture and the second in which the source is distributed across the fracture origin and the surrounding matrix. We assume the magnitude of thermal dispersivity is comparable to solute dispersivity. With this study, we show the potential error that accrues by neglecting longitudinal conduction and dispersion under naturally occurring hydraulic conditions (i.e. aperture and flow rate). In addition, we also demonstrate the effects of two dimensional matrix conduction in conjunction with dispersion and conduction in the fracture on two-dimensional conduction in heat transport in rock.

## 2.2 Theory

Both analytical and numerical models are used to explore heat transport in this study. The analytical solutions are developed by restricting conduction in the matrix to the direction perpendicular to the fracture. This is done because the derivation of an analytical model for the more general 2-D matrix conduction case is not easily tractable. Previous analytical derivations for this problem (Cheng et al., 2001; Baston and Kueper, 2009) have employed Green's functions and the Laplace Transform which lead to a

computationally demanding series solution with approximations for the inverse transform. In the present study, therefore we conduct the analysis in two steps whereby in the first step we look at the error induced by elimination of the dispersion term in the governing equation for the fracture ignoring the effect of 2-D conduction in the matrix, and in the second step we utilize a numerical model to address the same issue in the presence of 2-D matrix conduction.

To analytically model advective heat transport in a discrete fracture, three cases can be considered for the flowing fluid: (1) The general and most robust case with both conductive and dispersive heat transport in the fracture, (2) the non-dispersive (conductive) case with negligible dispersive transport in the fracture, and (3) the most widely used case with pure advection and negligible conductive and dispersive heat transport. To explore the effects of transverse dispersion in the fracture plane, the general case and the non-dispersive case are reevaluated using a two-dimensional analytical model. In the numerical section we consider two cases, with and without dispersion in the fracture. Heat is allowed to thermally conduct in both longitudinal and transverse directions in the matrix in the numerical model. The analytical model development, numerical model discretization, and the input parameters for both are described below.

### 2.2.1 Analytical Model

One-dimensional and two-dimensional analytical models are developed to explore heat transport in a single discrete fracture and fracture plane. In the following we explain the

conceptual models and their corresponding governing equations. The initial and boundary conditions and assumptions are also presented.

### *One-Dimensional Model*

The governing equation which describes heat transport in the fracture is given by (Yang et al., 1998):

$$\frac{\partial T}{\partial t} + v\frac{\partial T}{\partial z} - \frac{\lambda_z}{c_w \rho_w}\frac{\partial^2 T}{\partial z^2} - \frac{2\lambda_m}{c_w \rho_w 2b}\frac{\partial T'}{\partial x}\bigg|_{x=b} = 0 \qquad (1)$$

where $T$ is the temperature of the fracture fluid, $T'$ is the temperature in the surrounding rock matrix; $v$ is the uniform flow velocity of fracture fluid, $c_w$ is the specific heat of the fracture fluid, $\rho_w$ is the density of fracture fluid, $t$ is the elapsed time, $2b$ is the fracture aperture, $x$ represents the transverse direction, $z$ represents the longitudinal direction, $\lambda_m$ is the thermal conductivity of the matrix, and $\lambda_z$ is the effective thermal conductivity of the fracture fluid in the longitudinal direction. The parameter $\lambda_z$ includes the effects of thermal conduction through the fracture fluid as well as dispersion which occurs due to heterogeneity of the aperture in the fracture plane. In analogy to the hydrodynamic dispersion coefficient from solute transport, de Marsily (1986) proposed a similar expression for heat transport:

$$\lambda_z = \lambda_w + \alpha \rho_w c_w |v| \quad (2)$$

where $\lambda_w$ denotes the thermal conductivity of water and $\alpha$ represents the longitudinal thermal dispersivity (Bodin et al., 2003; Zhou et al., 2007). The thermal dispersion term is in a linear function of flow velocity.

For typical and more traditional studies, equation [1] is coupled with a one-dimensional equation which describes conductive heat transport in the matrix perpendicular to the orientation of the fracture (e.g. Gringarten et al., 1975; Bödvarsson and Tsang, 1982; Yang et al., 1998; Jung and Pruess, 2012; Gan and Elsworth, 2014):

$$\frac{\partial T'}{\partial t} - \frac{\lambda_m}{c_m \rho_m} \frac{\partial^2 T'}{\partial x^2} = 0 \quad (3)$$

where $c_m$ and $\rho_m$ are the specific heat and density of the rock matrix, respectively.

In the 1-D conductive analytical equation, dispersive transport in the fracture is neglected. The effective thermal conductivity, $\lambda$, is reduced to the thermal conductivity of water:

$$\lambda_z = \lambda_w \quad (4)$$

In order to compare to the other solutions, Yang et al. (1998) solution is provided here:

$$\bar{T} = \frac{T_0}{s}\exp(\gamma z)\exp\left\{-\gamma z\left[1+\beta^2\left(s+s^{1/2}/A\right)\right]^{1/2}\right\} \quad (5)$$

where $s$ is the Laplace parameter. $\bar{T}$ is the fracture temperature in the Laplace domain. $A$, $\gamma$ and $\beta$ are defined as:

$$A = \frac{bc_w\rho_w}{(\lambda_m c_m \rho_m)^{1/2}} \quad (6)$$

$$\gamma = \frac{v}{2\eta} \quad (7)$$

$$\beta^2 = \frac{4\eta}{v^2} \quad (8)$$

and:

$$\eta = \frac{\lambda_z}{c_w\rho_w} \quad (9)$$

For a detailed procedure of the derivation of equation [5], please refer to Yang et al. (1998).

***Two-Dimensional model***

The conceptual model for two-dimensional heat transport in a fracture is shown in Figure 1. For the fracture equation, we consider advective, conduction and dispersive transport of heat in the $z$ direction within the fracture plane. In this case the lateral spreading of heat in the y direction is also considered in the fracture equation. The same

matrix equation is used as in the 1-D solution expressed by equation [3] where transport of heat is dominated by conduction along the vertical x-axis.

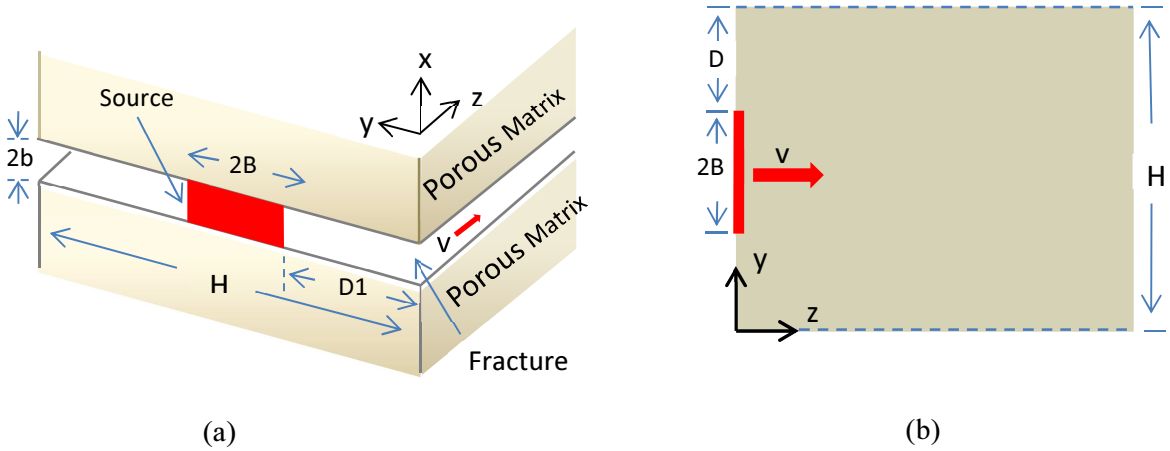


(a) (b)

**Figure 1: (a) Two-dimensional fracture-matrix system. The matrix extends to infinity in both x and z directions. (b) Plan view of the fracture in the y-z plane, the system is confined with no flux boundaries in the y direction.**

In the literature at present, none of the existing two dimensional analytical models have considered lateral transport of heat within the fracture plane. The two-dimensional heat transport equation used in this study is modified from the solute transport equation developed by West et al. (2004), given that the mathematical expression for heat transport is similar to solute transport in discrete fracture studies.

The equation governing heat transport in the fracture is given by:

$$\frac{\partial T}{\partial t} + v\frac{\partial T}{\partial z} - \frac{\lambda_z}{c_w\rho_w}\frac{\partial^2 T}{\partial z^2} - \frac{\lambda_y}{c_w\rho_w}\frac{\partial^2 T}{\partial y^2} - \frac{\lambda_m}{c_w\rho_w b}\frac{\partial T'}{\partial x}\bigg|_{x=b} = 0 \qquad (10)$$

where the first term at the left hand side represents heat storage, the second term represents the advective transport of heat in the $z$ direction, the third term represents

conductive and dispersive transport of heat in the *z* direction, the forth term represents transverse conduction and dispersion in the *y*-*z* plane, and the fifth term represents heat lost into the matrix through conduction.

The initial and boundary conditions for equation [10] are given as:

$$T(x, y, z, 0) = 0 \tag{11}$$

$$T(x, y, \infty, 0) = 0 \tag{12}$$

$$T(x, y, 0, t) = T_0 \delta(y - y') \tag{13}$$

$$\frac{\partial T}{\partial y}(x, 0, z, t) = 0 \tag{14}$$

$$\frac{\partial T}{\partial y}(x, H, z, t) = 0 \tag{15}$$

In contrast to the 1-D general equation (equation [1]) the two-dimensional general equation (equation [10]) introduces an additional transport mechanism in the *y* direction within the fracture plane. This allows heat to migrate laterally within the fracture plane under the influence of transverse conduction and dispersion.

### 2.2.2 Analytical Solutions

There are three cases considered for the 1-D model and two cases for the two-dimensional model. For the 1-D solutions, we will first present the solution for the general case, followed by the non-dispersive (conductive) case with thermal dispersivity

($\alpha$) equals to zero, and finally, we develop the solution for the advection only case by neglecting effective thermal conductivity ($\lambda_z$). These three solutions are compared to study the effects of conduction and dispersion, and the procedure is explained in the method section below.

For the 2-D problem, solutions are developed for the general and the conductive cases. The two-dimensional conductive solution is compared to the two-dimensional general solution to explore the effects of dispersion in a fracture plane. All the solutions are solved in the Laplace space and then numerically inverted using the MATLAB routine programmed by Hollenbeck (1998) based on the de Hoog et al. (1982) algorithm. This inversion routine has been tested and verified against other inversion methods (i.e. the Stehfest, the Zakian, the Honig-Hirdes, and the Talbot methods) by Wang and Zhan (2015) and has been applied to accurately solve groundwater flow and transport problems (i.e. Bader and Kooi, 2005; Audouin and Bodin, 2008).

***One-Dimensional Model***

The general solution for equation [1]-[3] is given in equation [5]. The conductive solution shares the same form as the general solution but with the effective thermal conductivity equals to the conductivity of water, equation [4]. For the advection only solution, we neglect both conduction and dispersion in the fracture transport equation, thus the governing equation is reduced to a first-order partial differential equation:

$$\frac{\partial T}{\partial t} + v\frac{\partial T}{\partial x} - \frac{2\lambda_m}{c_w \rho_w 2b}\frac{\partial T'}{\partial z}\bigg|_{x=b} = 0 \qquad (16)$$

Equation [16] cannot be solved by simply removing the conduction term from the 1-D general solution, equation [5], as mathematic error occurs when assigning zero value to the conductivity of water $\lambda_w$. Therefore, a full solution is derived by applying the same initial and boundary conditions as used in Yang et al (1998). The solution in the Laplace domain is expressed as:

$$\bar{T} = \frac{T_0}{s}\exp\left\{-\frac{z}{v}\left[s + \frac{s^{1/2}}{A}\right]\right\} \qquad (17)$$

where $s$ is the Laplace variable and $A$ is defined in equation [6].

***Two-Dimensional Model***

The two-dimensional fracture equation [10] is first solved in Laplace and Fourier spaces and subsequently inverted using an inverse finite cosine Fourier transform, integrated with respect to source geometry, and finally numerically inverted using the routine by Hollenbeck (1998). Two cases are considered for the flowing fluid; the general case with conductive and dispersive heat transport in the $y$ and $z$ directions in the fracture plane, and a case with negligible dispersion. For both cases, a heat source having a width of $2B$ is located in the fracture plane.

The two-dimensional general solution in Laplace space that describes transient temperature change in the fracture is given as:

$$\overline{T}(x,y,z,s)$$
$$= \frac{2BT_0}{Hs}\exp\left(\frac{vz}{2\eta}\right)exp\left[-z\sqrt{\frac{v^2}{4\eta^2}+\frac{1}{\eta}\left(s+\frac{s^{1/2}}{A}\right)}\right]$$
$$+\frac{2T_0}{s}\exp\left(\frac{vz}{2\eta}\right)\sum_{n=1}^{\infty}\frac{1}{n\pi}\cos\left(\frac{n\pi y}{H}\right)\left\{\sin\left[\frac{n\pi(D_1+2B)}{H}\right]-\sin\left(\frac{n\pi D_1}{H}\right)\right\}$$
$$\times\exp\left\{-z\sqrt{\frac{v^2}{4\eta^2}+\frac{\lambda_y}{\lambda_z}\frac{n^2\pi^2}{H^2}+\frac{1}{\eta}\left(s+\frac{s^{1/2}}{A}\right)}\right\} \qquad (18)$$

where $s$ is the Laplace variable, $A$ is defined in equation [6], and $\eta$ is defined in equation [9].

Thermal dispersion and conduction in the longitudinal direction $\lambda_z$ is given in equation [2] and the transverse direction $\lambda_y$ is given by:

$$\lambda_y = \lambda_w + \alpha_y\rho_w c_w|v| \qquad (19)$$

Verification of the 2-D general solution, equation [18], was performed by comparison with the 1-D general solution, equation [5] with equation [2]. In the verification, $\lambda_y$ is set to a negligible value which forces the two-dimensional transport in the fracture plane to a 1-D problem. Then temperature along the fracture is simulated at fracture aperture,

*2b*= 1000 μm, and flow velocity of 11.6 x $10^{-4}$ m/s (100 m/day). The maximum temperature difference between the two solutions was calculated to be no more than 5.0 x $10^{-15}$ °C. Similar differences were observed between the two solutions at different apertures and velocities.

Similarly, the two-dimensional conductive solution which neglects dispersive transport in both the longitudinal and transverse directions in the fracture plane is given as:

$$\overline{T}(x,y,z,s) = \frac{2BT_0}{Hs}\exp\left(\frac{vz}{2\eta}\right)exp\left[-z\sqrt{\frac{v^2}{4\eta^2}+\frac{1}{\eta}\left(s+\frac{s^{1/2}}{A}\right)}\right]$$
$$+\frac{2T_0}{s}\exp\left(\frac{vz}{2\eta}\right)\sum_{n=1}^{\infty}\frac{1}{n\pi}\cos\left(\frac{n\pi y}{H}\right)\left\{\sin\left[\frac{n\pi(D_1+2B)}{H}\right]-\sin\left(\frac{n\pi D_1}{H}\right)\right\}$$
$$\times\exp\left\{-z\sqrt{\frac{v^2}{4\eta^2}+\frac{n^2\pi^2}{H^2}+\frac{1}{\eta}\left(s+\frac{s^{1/2}}{A}\right)}\right\} \quad (20)$$

Assuming dispersive transport in the fracture is negligible, thus $\eta$ simplifies to the thermal diffusivity of water which is given as:

$$\eta = \frac{\lambda_w}{c_w\rho_w} \quad (21)$$

A detailed derivation of this solution follows the solution method for solute transport published by West et al. (2004). Similar derivation method is used in the unpublished work by André and Sudicky (1991).

Verification of the two-dimensional conductive solution, equation [20], was performed in a similar manner to the verification of the 1-D general solution. The two-dimensional conductive solution is compared with the 1-D advection only solution, equation [17]. In the verification, the conductivity of water $\lambda_w$ is set to a negligible value which forces the two-dimensional solution become one-dimensional. The maximum temperature difference between the two solutions is calculated to be $4 \times 10^{-13}$ °C at a fracture aperture of 1000 μm and flow velocity of $11.6 \times 10^{-4}$ m/s (100 m/day). Again similar agreement was observed between the two solutions at different aperture and velocities.

### 2.2.3 Numerical Model

To study the effects of longitudinal matrix conduction on the significance of dispersion in the fracture, we use a numerical model, HydroGeoSphere (HGS), a three-dimensional control-volume finite element package which is capable of simulating coupled hydrological and thermodynamic transport processes in both fractured and porous environments (Therrien et al., 2010). HydroGeoSphere has recently been used to simulate the performance of enhanced geothermal systems and ground heat exchangers (Doe et al., 2014; Raymond and Therrien, 2014; Simms et al., 2014).

Figure 2 shows a schematic diagram of the two-dimensional grid that was implemented in HydroGeoSphere. A single discrete fracture is located at the center of the domain along the z-axis. Two types of heat sources with constant temperature of 10 °C are considered in the numerical model. This includes a point source located in the fracture and a line source which varies from 0.1 m to 6.0 m in length along the x-axis. This line source represents a heating element which could be a wellbore or a repository in a natural setting. A type I hydraulic boundary condition (e.g. constant pressure at any time step) is used at the top and bottom of the model. This creates an upward flow in the fracture. No flow boundary conditions are used at the left and right sides. A value of $1.0 \times 10^{-40}$ m/s for the hydraulic conductivity was used for the rock matrix to eliminate flow in this part of the system. The model is initialized with a uniform temperature of 0 °C. Adiabatic boundary conditions are used on all four sides. Temperature at the elements near the top, left and right boundaries were continuously monitored for all the simulations to avoid reflection boundary effects. The maximum change in temperature at the boundary elements was observed to be no more than $1.0 \times 10^{-3}$ °C.

Different discretization and domain sizes are defined at two aperture scenarios. For the large aperture scenario, the model has a dimension of 30 m by 30 m in the *x* and *z* directions. The discretization in the z direction starts at 0.01 m at the bottom elements and gradually increases to 0.1 m near the top. The horizontal refinement starts at 0.01 m in the vicinity of the fracture and gradually increases to 0.2 m in both directions. For the small aperture scenario where the thermal front is expected to propagate slower, a smaller domain was used. The domain has a width of 16 m and a length of 10 m. The grid shown

in Figure 2 is provided for illustration and is courser by a factor of approximately 10 than the actual grids that were used in the simulations. The discretization starts at 0.001 m and gradually increases to 0.08 m in the *z* direction and starts at 0.001m adjacent to the fracture and increases to 0.08 m at the lateral boundaries. The extremely fine discretization in the *z* direction ensures the model accuracy to at least the second significant figure, as shown below.

Verification of the numerical model was done by comparison with the one-dimensional general solution using an aperture of 300 μm, a flow velocity of $5.0 \times 10^{-3}$ m/s (432 m/day) and an injection temperature of 10 °C. An unrealistically high flow velocity was selected to minimize the effects of matrix conduction. In the advection dominant region (i.e. the fracture), the temperature estimated by both solutions agrees to two decimal places indicating the accuracy of the numerical model. In order to control the error propagated by time stepping in the simulations, the maximum allowed absolute change in nodal temperature is set as 0.5 °C during any time step.

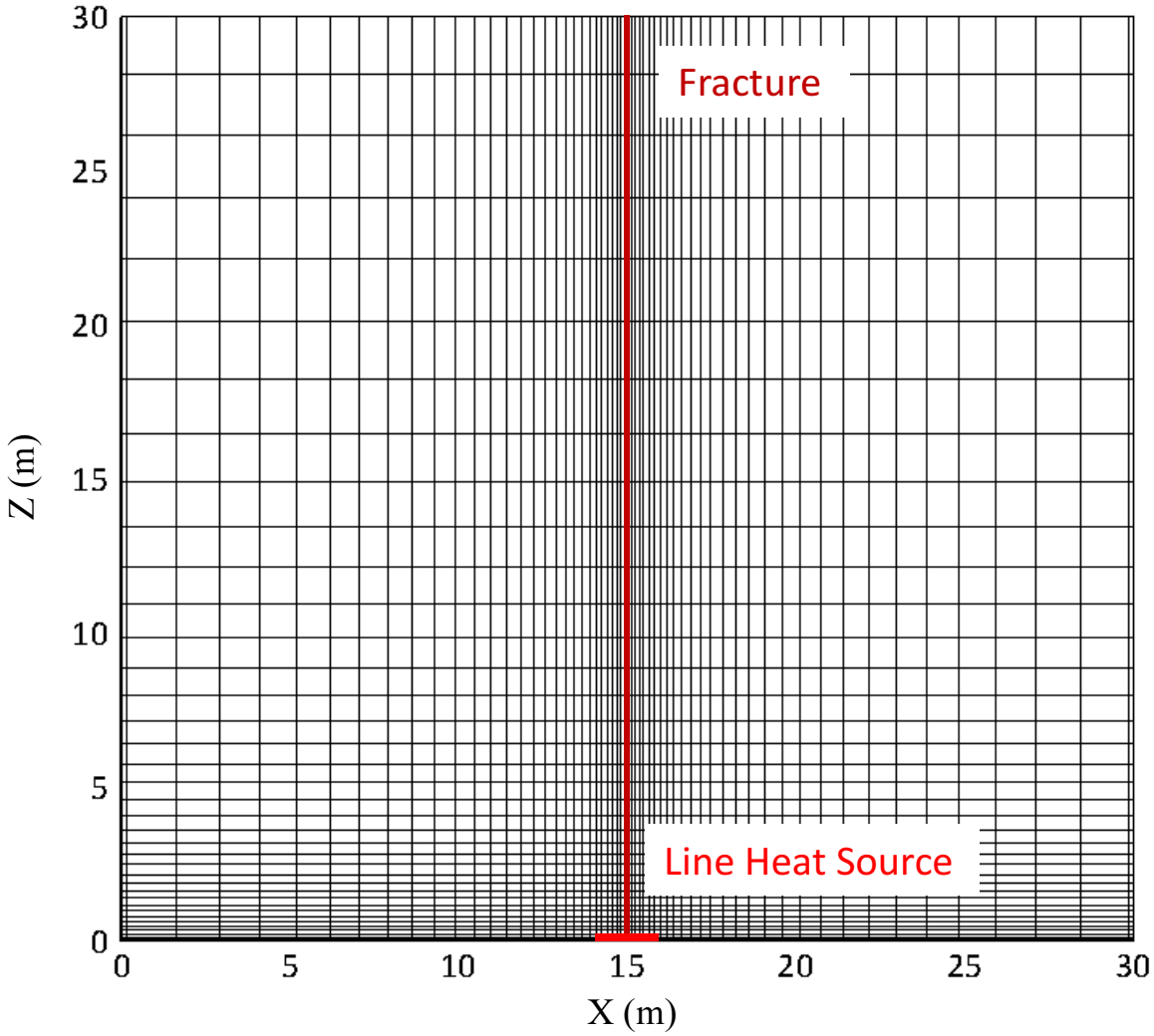


**Figure 2: Grid for the two-dimensional numerical model with a discrete fracture. For the large aperture case, the model dimension is set to 30 m by 30 m. For the small aperture case, the dimension is set to 16 m by 10 m in the x-and z-directions, respectively. The grid is shown for illustration. The actual grid is much finer (starting from 0.001 m in the vicinity of the fracture and gradually increasing to 0.1 m in the x-direction).**

## 2.3 Method

The first step in the modeling is to illustrate the importance of 3-D heat conduction in the matrix. This is done using a comparison between 1-D analytical solution for conduction in the plane of the fracture and 1-D conduction in the matrix (equation [5] with equation [4]) to the numerical model for the same conditions except 2-D conduction in the matrix is accommodated. Secondly, we show the results from the 1-D analytical solutions where we compare the advection-only solution (equation [17]) with the 1-D conduction solution (equation [5] with equation [4]) to study the effects of longitudinal thermal conduction in the fracture. The effects of longitudinal dispersion were examined by comparison between the 1-D conductive solution (equation [4]) with the 1-D general solution (equation [2]) using equation [5]. Thirdly, we present the results from the two-dimensional model, where the effect of both longitudinal and transverse dispersion is evaluated by comparison between equation [18] and equation [20]. Finally, we present the results from the numerical analysis in which we consider 2-D conduction in in the matrix and longitudinal conduction and dispersion in the fracture.

This section also summarizes the hydraulic and thermal transport parameters that were used in the modeling. Two groups of thermal dispersivity values are selected based on the physical scales of the problems. The methods that were used to analyze the differences between solutions are also explained.

### 2.3.1 Input Parameters

Table 1 summarizes the eight thermal transport parameters used for the modeling. In the 1-D and 2-D analytical models, fluid with a constant temperature of 1 °C is injected into the fracture. A higher injection temperature of 10 °C is set in the numerical model. The higher injection temperature reduces the numerical instability and thus increases the model accuracy. The temperature is 0 °C everywhere in the system prior to the heated fluid injection. The matrix is assumed to have the property of shale with heat conductivity of 2.0 W/m °C, specific heat of 800 J/kg °C, and a density of 2650 kg/m$^3$ (Côté et al., 2012). Thermal parameters are assumed to remain constant through the analyses as the injection temperature is only 1-10 °C higher than the initial temperature in the domain. This simplification can be justified by the sensitivity analysis performed by Baston and Kueper (2009) in which it was concluded that the variations in thermal properties play a minor role in simulating heat transport in fracture systems.

**Table 1: Thermal transport properties and initial conditions**

| Parameter | Unit | Value |
|---|---|---|
| Injection temperature | °C | 1.0-15.0 |
| Initial temperature | °C | 0.0 |
| **Matrix Properties** | | |
| Thermal conductivity ($\lambda_m$) | (W/m°C) | 2.0 |
| Specific heat ($c_m$) | (J/kg °C) | 800 |
| Density ($\rho_m$) | ($kg/m^3$) | 2650 |
| **Fluid (water) Properties** | | |
| Thermal conductivity ($\lambda_w$) | (W/m°C) | 0.5 |
| Specific heat ($c_w$) | (J/kg °C) | 4174 |
| Density ($\rho_w$) | ($kg/m^3$) | 1000 |

Two cases are selected to illustrate the effects of longitudinal conduction and dispersion. The large aperture case consists of $2b$ = 1000 μm and the flow velocity ranges between 2.3 x $10^{-5}$ m/s (2 m/day) and 4.6 x $10^{-4}$ m/s (40 m/day). The small aperture case consists of $2b$ = 100 μm and the flow velocity ranges between 5.8 x $10^{-6}$ m/s (0.5 m/day) and 1.2 x $10^{-4}$ m/s (10 m/day). These ranges of aperture and flow velocity parameters are selected based on field measurements performed in naturally occurring single fractures and thus should be representative of the range of these parameters in a natural setting (Tang et al., 1981; West et al., 2004; Novakowski et al., 2006; Zhou et al., 2007; Bagalkot and Kumar, 2014).

To the best of the author's knowledge, in the literature at present there are no laboratory or field scale experiments which have been performed to measure thermal dispersivity ($\alpha$)

in single fracture settings. In this study, we assume $\alpha$ is comparable to solute dispersivity and occurs through approximately the same physical processes (for example, due to aperture heterogeneity, closure, and fracture wall roughness). Based on tracer experiments conducted in discrete fractures under natural groundwater flow conditions, it is observed that dispersivity increases as a function of the fracture length (Guimera and Carrera, 2000). As the field scale increases from 3.0 m to 45 m in published reviews and field studies, longitudinal dispersivity increases from 0.1 m to 10 m and the transverse dispersivity is assumed to approximate 10 percent of the corresponding longitudinal dispersivity (Gelhar et al., 1992; Lapcevic et al., 1999; Bodin et al., 2003). In this study, we set the dispersivity values according to the length of fractures. In the one-dimensional analytical analyses, a fracture with a length of 3.0 m is simulated for 150 days. Considering the short length of the fracture, longitudinal dispersivity is set to 0.1 m. Similarly in the two-dimensional analyses with analytical solution, the dispersivities are set to $\alpha_z$ = 0.1 m and $\alpha_y$ = 0.01. Finally for the numerical solution, a 15 m long discrete fracture is simulated for 250 days. Considering the length of the fracture, longitudinal dispersivity is assumed to equal 1.0 m.

### 2.3.2 Heat Front and Error

The heat front location ($Z_f$) is calculated to make comparison between the previously described solutions. The position of heat front is defined as the distance along the fracture centerline at which the temperature equals 0.01 °C at any given time. The value of 0.01 °C was selected as the definition of the heat front because the measurement of very low

temperature changes is now possible with high resolution thermistors (typical accuracy of ±0.002 °C). For the estimation of hydraulic properties between boreholes using heat transport (eg. Klepikova et al., 2014), analysis of very small temperature changes will be necessary. The heat front calculated from the numerical modelling is defined at a higher temperature of 1 °C. This is because the injection temperature is 9 °C higher than used in the analytical models. It was also observed that the numerical results became unstable for a heat front value below 1 °C. Unreasonably fine discretization and a substantial increase in the number of time steps would be required to bring down the heat front estimate to anything near that possible with the analytical models. This is a significant limitation to the use of numerical models for the analysis of heat transport in fractured media.

Comparisons between solutions are performed based on the computed error which estimates the differences between the approximated heat front and true heat front. The error is expressed as:

$$Error\ (\%) = \frac{(Z_f^t - Z_f^a)}{Z_f^t} * 100 \tag{22}$$

in which $Z_f^t$ represents the position of the true heat front, and $Z_f^a$ represents the approximate heat front. For example, Figure 3 depicts the temperature along the fracture at 5 days given by the 1-D general solution and the 1-D conductive solution. In order to quantify the discrepancies between the two solutions, percentage error can be calculated

using equation (22), in which the true value corresponds to the dispersive front, and the approximate value corresponds to the conductive front.

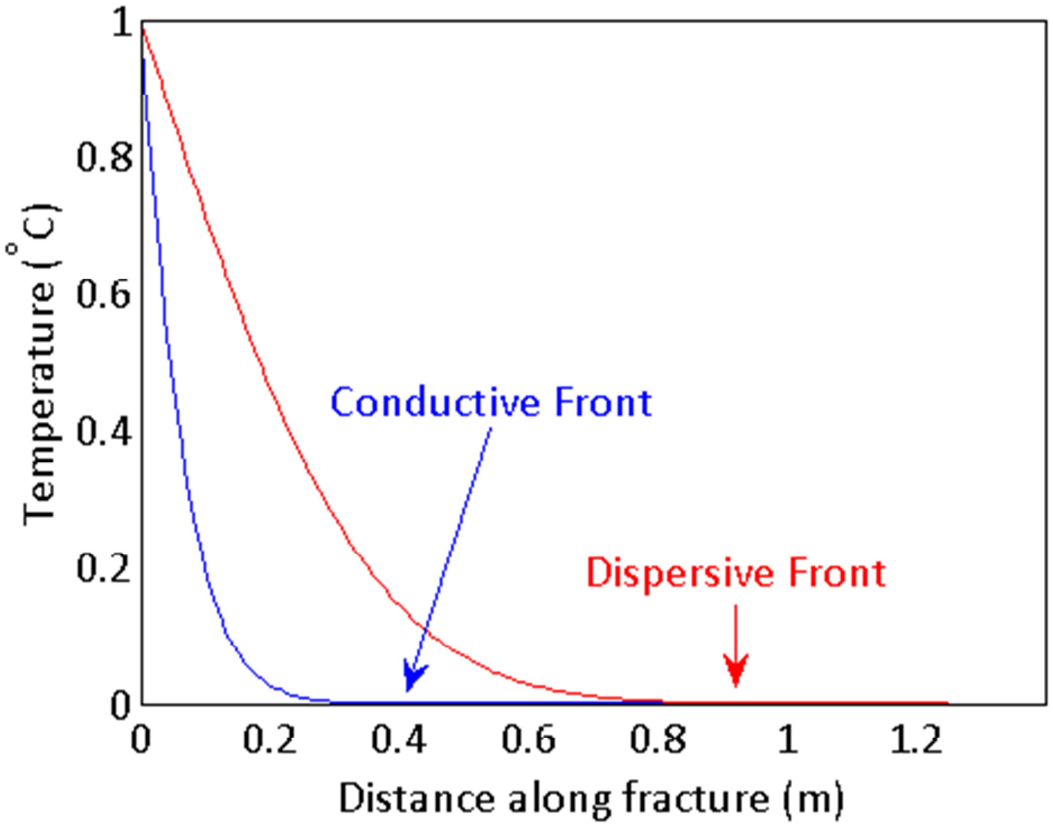


**Figure 3: Temperature along the fracture at 5 days given by the 1-D general solution (red) and the 1-D conductive solution (blue), at aperture= 500 μm, flow velocity= 5 m/day and an injection temperature of 1 °C.**

## 2.4 Results and Discussion

The previously described analytical and numerical models were used to explore the effects of longitudinal conduction and dispersion using the fracture heat transport equation. The percentage error which occurs by neglecting conduction and dispersion is discussed for a large and small aperture cases.

### 2.4.1 Effects of Matrix Conduction

As aforementioned, the analytical solutions that were used in this study neglect longitudinal conduction in the matrix. This simplification may cause deviation between the analytical results and the most accurate and representative values (e.g. the numerical results in which both transverse and longitudinal conduction are considered). In order to demonstrate the effects of longitudinal conduction in the matrix, the 1-D conductive solution is compared with the numerical solution. Figure 4 shows the 1 °C temperature contours that were obtained using the 1-D conductive solution and the numerical solution at 50 and 150 days. A vertical fracture with an aperture of 1000 μm is located at X=15 m. Water flows into the fracture with an initial temperature of 15 ºC and a constant flow rate of 50 m/day. Figure 4 shows that the conductive solution significantly underestimates the lengths of the plumes in the z-direction and overestimates the widths of plumes in the x-direction. This observation agrees with previous studies which have recently suggested that longitudinal conduction in the matrix enhances heat propagation in the longitudinal direction (Li, 2014; Ruiz Martínez et al., 2014).

Although heat transport in the fracture is the focus of this study, longitudinal conduction in the matrix is an important process to consider as suggested by the results shown in Figure 4. It is possible that longitudinal conduction in the matrix will either enhance or diminish the effects of longitudinal heat dispersion in the fracture. To study the effects of longitudinal conduction in the matrix on the conduction and dispersion in the fracture, comparison between the numerical results and the analytical results were performed as described in Section 2.4.3.

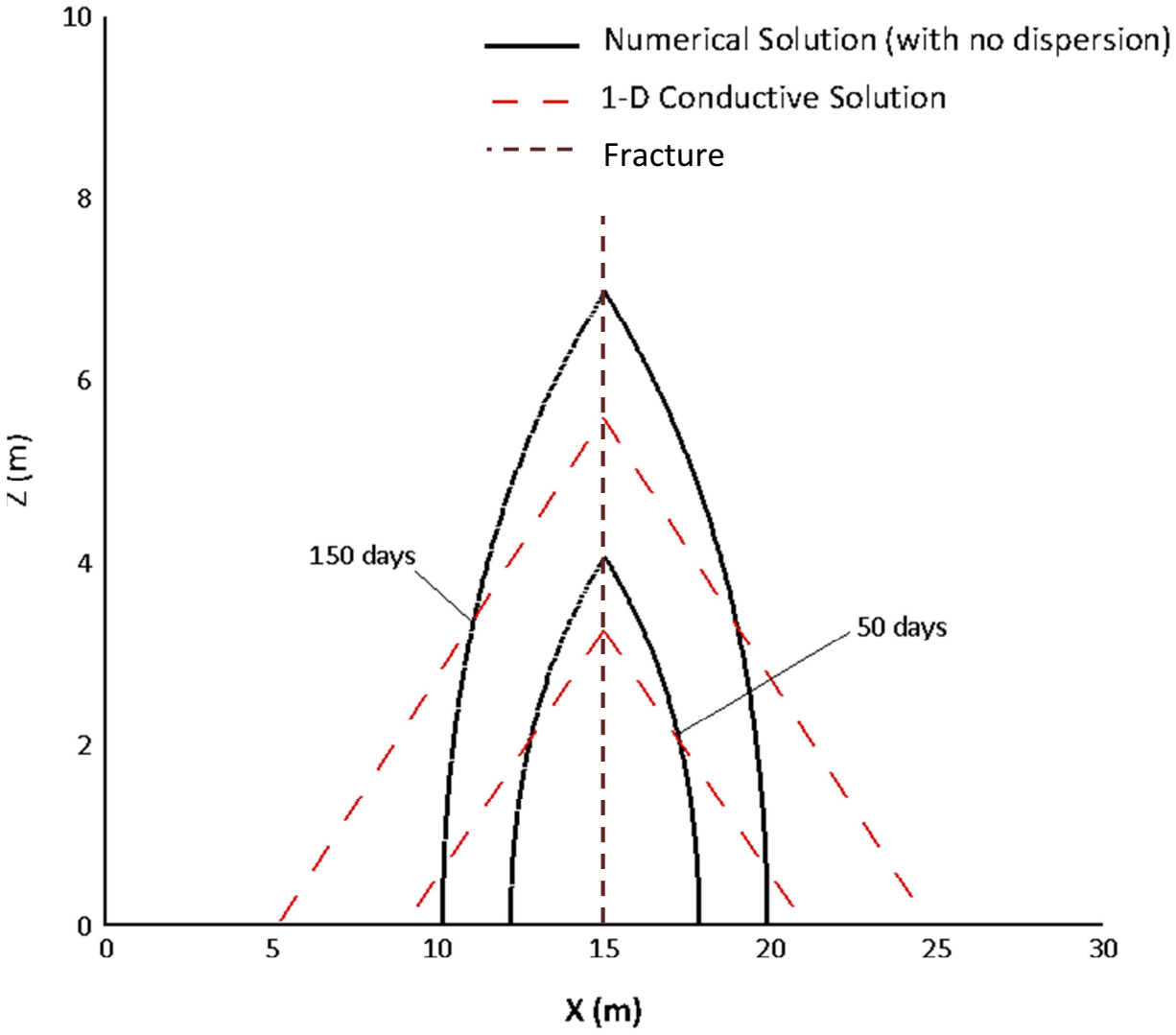


**Figure 4: Comparison between the conductive solution (red) versus the numerical solution (blue) for a 1 °C temperature contour in the domain, aperture, 2b =1000 µm, flow velocity, v = 50 m/day and injection temperature 15 °C.**

### 2.4.2 Significance of Longitudinal Conduction in the Fracture

To assess the discrepancies between the conductive and the advective-only solution, the percentage heat front differences are plotted in Figure 5. A large error would suggest that the effects of longitudinal conduction in the fracture are significant and therefore should

not be neglected from the heat transport equation. A large aperture, *2b*=1000 μm, and a small aperture, *2b*=100 μm, are selected and discussed below.

Figure 5 (a) shows the error of neglecting longitudinal conduction at an aperture of 100 μm. As the flow velocity decreases from 4 m/day to 0.5 m/day, the error increases to almost 100%. This substantial amount of error indicates that the system is conduction dominant; therefore, longitudinal conduction should be considered in the fracture heat transport equation in this case.

Comparing Figure 5(a) with Figure 5(b), the error is higher for the small aperture case. For example, at aperture 2b=100 μm and flow velocity v = 2 m/day, neglecting thermal conduction yields error from 70% to 85%. For the large aperture case, same flow velocity yields error from 20% to 65%. Comparison between the large and small aperture cases suggests that, given the same flow velocity, thermal conduction is more significant in small aperture settings.

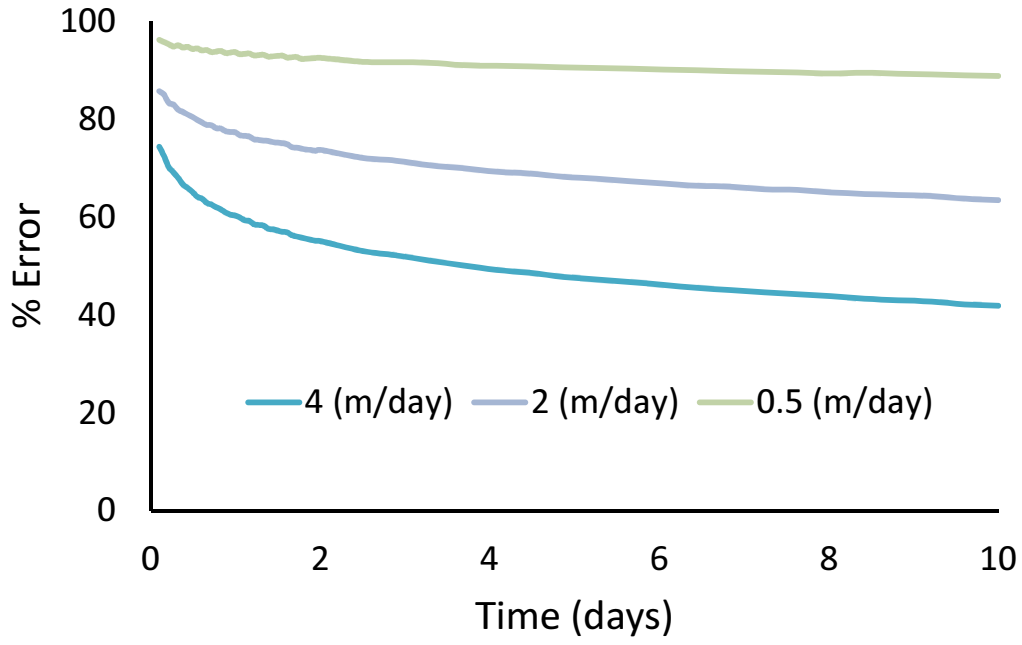


(a) large aperture *2b*=1000 µm

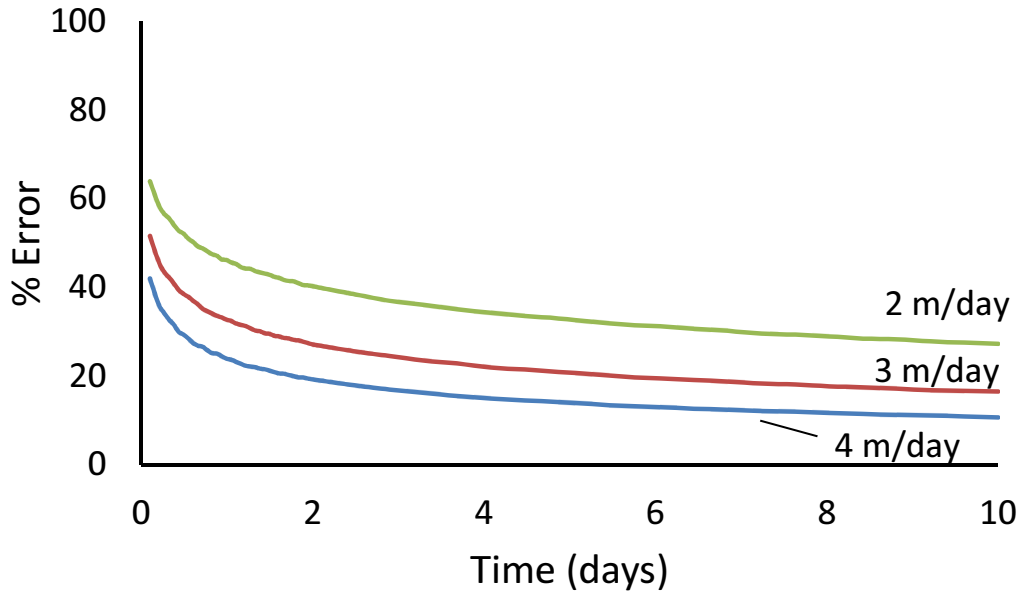


(b) small aperture *2b*=100 µm

**Figure 5: Error in heat front position due to neglecting longitudinal thermal conduction in 1-D heat transport in a fracture. (a) Small Aperture 2b=100 µm, (b) Large Aperture 2b=1000 µm.**

### 2.4.3 Significance of Longitudinal Dispersion in the Fracture

In this section we discuss the percentage error due to neglecting dispersive transport in the fracture heat transport equation. The previously described 1-D analytical solution, 2-D analytical solution and numerical solution are used to simulate heat transport in the fracture. The effects of longitudinal conduction in the matrix are also discussed.

**One-Dimensional Heat Transport in the Fracture**

To assess the influences of longitudinal dispersion, a series of analyses have been performed in comparing the 1-D general solution (considering both dispersion and conduction in the fracture) with the 1-D conductive solution (neglecting dispersion in the fracture). The magnitude of the longitudinal thermal dispersion coefficient ($\alpha$) is assumed to be comparable to the solute dispersion coefficient, and a value of 0.1 m is used throughout the 1-D analyses.

Figure 6 (a) and Figure 6 (b) show the errors due to neglecting longitudinal dispersion for large and small aperture cases, respectively. In general, the errors start high and decrease over time. Comparing Figure 6 (a) and Figure 6 (b), the errors are higher at the small aperture case where they are greater than 60% at 150 days. We also calculated energy balances by integrating the thermal energy that was stored in the fracture, and the results were similar to the heat front analyses. The significant amount of error indicates that dispersion in the fracture is important and should be included in the heat transport

equation for the fracture. Neglecting dispersion would underestimate the location of the heat front by at least 20% and leads to significant error in the energy balance.

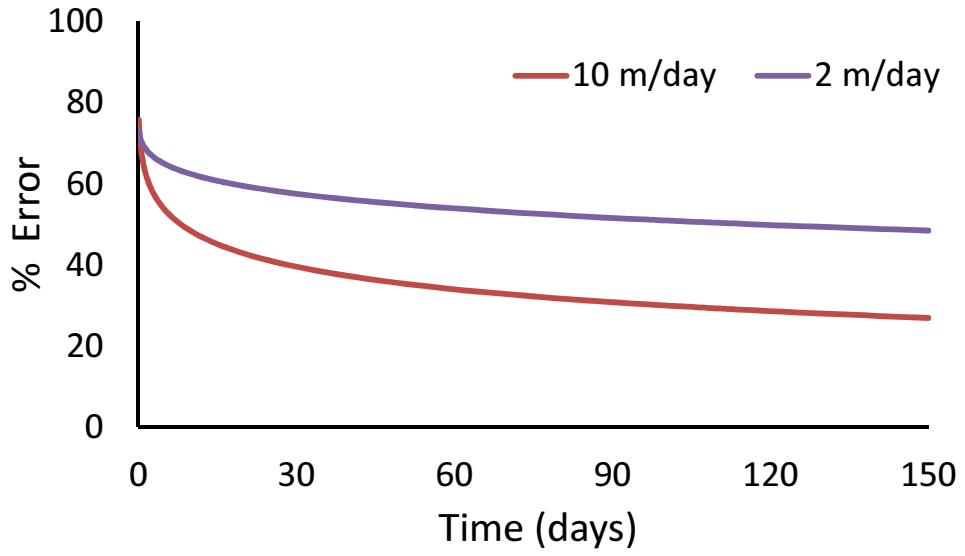


(b) large aperture *2b*=1000 μm

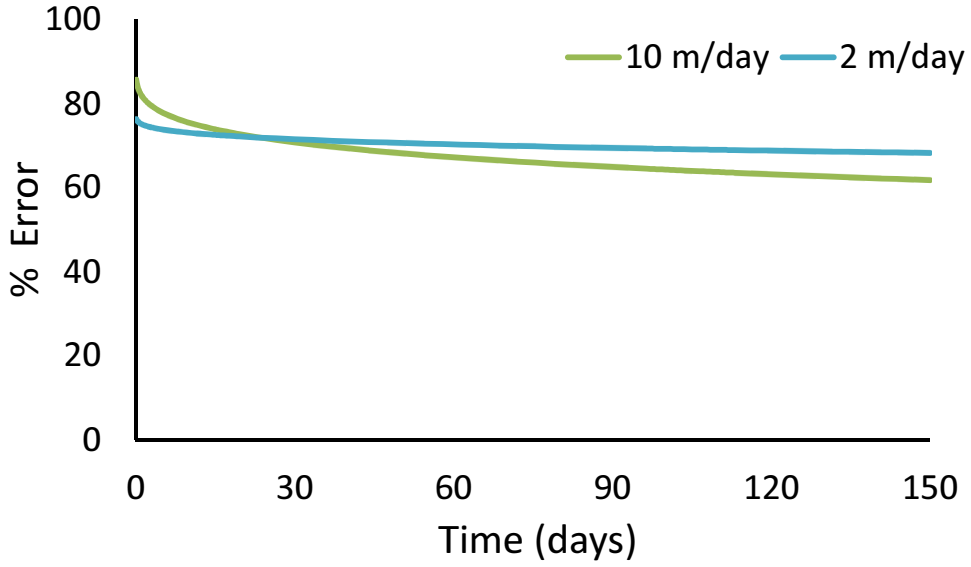


(b) Small aperture *2b*=100 μm

**Figure 6: Error in heat front position due to neglecting dispersion in 1-D heat transport in a fracture. (a) Large Aperture 2b=1000, (b) Small Aperture 2b=100. Thermal dispersivity ($\alpha$) equals to 0.1 m.**

### *Two-Dimensional Heat Transport in the Fracture*

A 2-D parallel plate model is used to study the effects of longitudinal and transverse dispersion in the fracture plane. Although these effects may be swamped by 2-D conduction in the matrix particularly at smaller aperture, and low velocity, it is significantly easier to explore transverse dispersion using an analytical model with 1-D matrix conduction. Therefore, in this case we chose to explore the effects of dispersion using analytical solution which considers 2-D transport in the fracture plane and 1-D conduction in the matrix.

To demonstrate the effects of transverse dispersion, the 2-D dispersion solution, equation [18], is compared with the 2-D conduction solution, equation [20], both of which were derived for the plane of the fracture. For the 2-D dispersion solution, we consider dispersion and conduction in both longitudinal and transverse directions within the fracture plane. Longitudinal and transverse dispersivity values are set as $\alpha_z$= 0.1 m and $\alpha_y$= 0.01 m respectively. In contrast, the 2-D conduction solution neglects dispersive transport in both directions. The 2-D conduction solution can be seen as a special case of the 2-D dispersion solution by setting the dispersivity values to zero ($\alpha_z$= 0 m $\alpha_y$= 0 m). The locations of the heat front were calculated and compared between the two solutions.

Figure 7 shows the 0.01ºC temperature contours in the fracture plane (Y-Z Plane). The heat fronts are located along the center line of the fracture plane where Y = 0 m. At day 5, the dispersive front is ahead of the conductive front. This indicates that the conductive solution, equation [20], underestimates the movement of the heat front at

early time (less than five days). However, the dispersive front slows down and meets the conductive front at day 40. At day 1000, the transverse dispersion significantly retards the front movement which results in an oblong-shaped plume. Comparing the conductive plume to the dispersive plume at 1000 days, the conductive solution overestimates the length and underestimates the width of the plume.

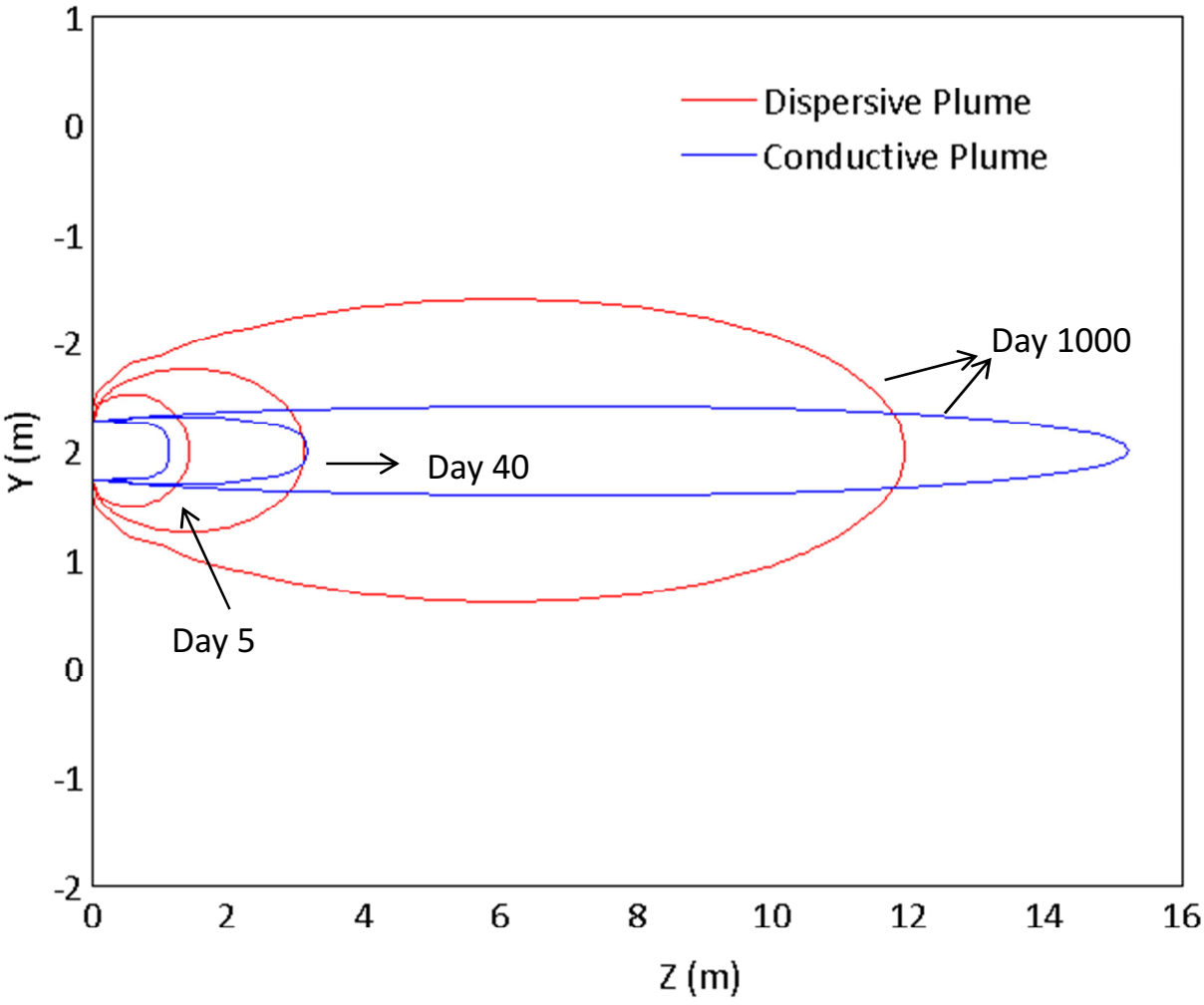


**Figure 7: The 0.01 °C temperature contour obtained from the 2-D dispersive solution, equation [18], and the 2-D conductive solution, equation [20], in the plane of the fracture. The flow velocity equals 40 m/day, and fracture aperture equals 1000 μm.**

Figure 8 shows the error due to neglecting dispersion at a velocity $v$= 40 m/day and an aperture $2b$=1000 µm with dispersivity values of $\alpha_z$= 0.1 m and $\alpha_y$= 0.01 m. At early time (less than 40 days), neglecting dispersion in the fracture plane yields positive error up to 40%. The sign of the error switches from positive to negative after 40 days. This change is due to the movement of the dispersive front which is significantly retarded by dispersion in the lateral direction (along the Y axis). Thus for this case, dispersion is a critical phenomenal that governs heat transport in the fracture plane. The conductive solution which neglects dispersion underestimates the heat front location at early time (less than 40 days) and overestimates the heat front location after 40 days.

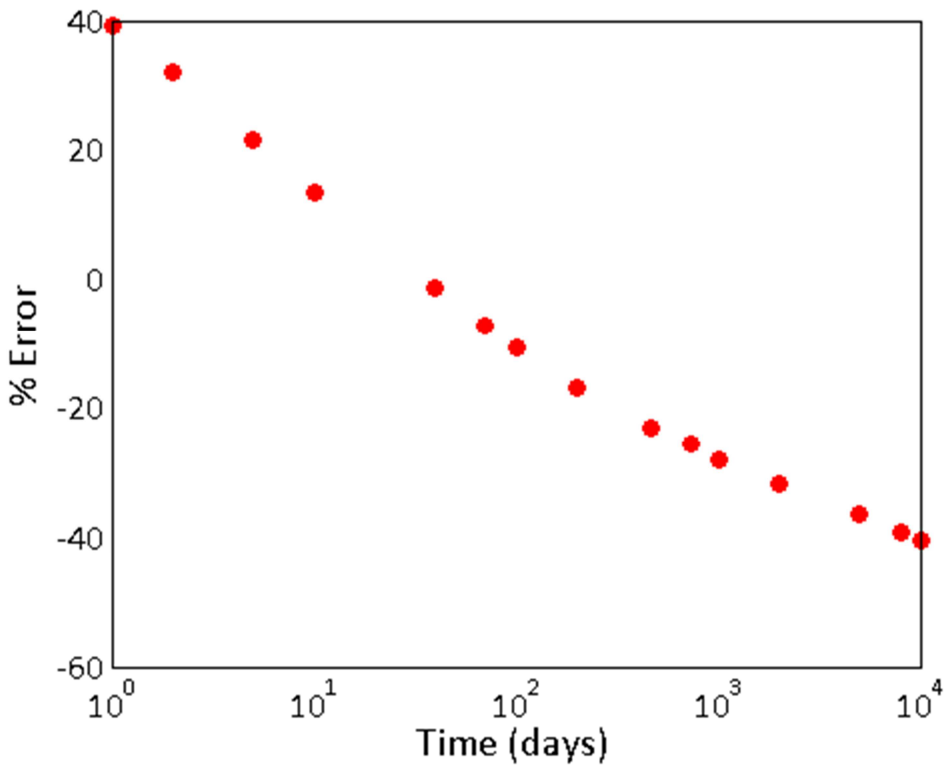


**Figure 8: Error in the heat front position due to neglecting thermal dispersion in 2-D heat transport in the plane of the fracture. Longitudinal dispersivity $\alpha_z$= 0.1 m, transverse dispersivity $\alpha_y$= 0.01 m, $2b$= 1000 µm, and $v$= 40m/day.**

Figure 9 shows the error due to neglecting dispersion at velocity $v$= 1 m/day and aperture $2b$=100 µm with dispersivity values of $\alpha_z$= 0.1 m and $\alpha_y$= 0.01 m. At small aperture and low flow rate, the conductive solution underestimates the location of heat front. However, these results are likely to be more strongly influenced by 2-D conduction in the matrix than those at larger aperture and higher velocity. This is explored more thoroughly in the following section.

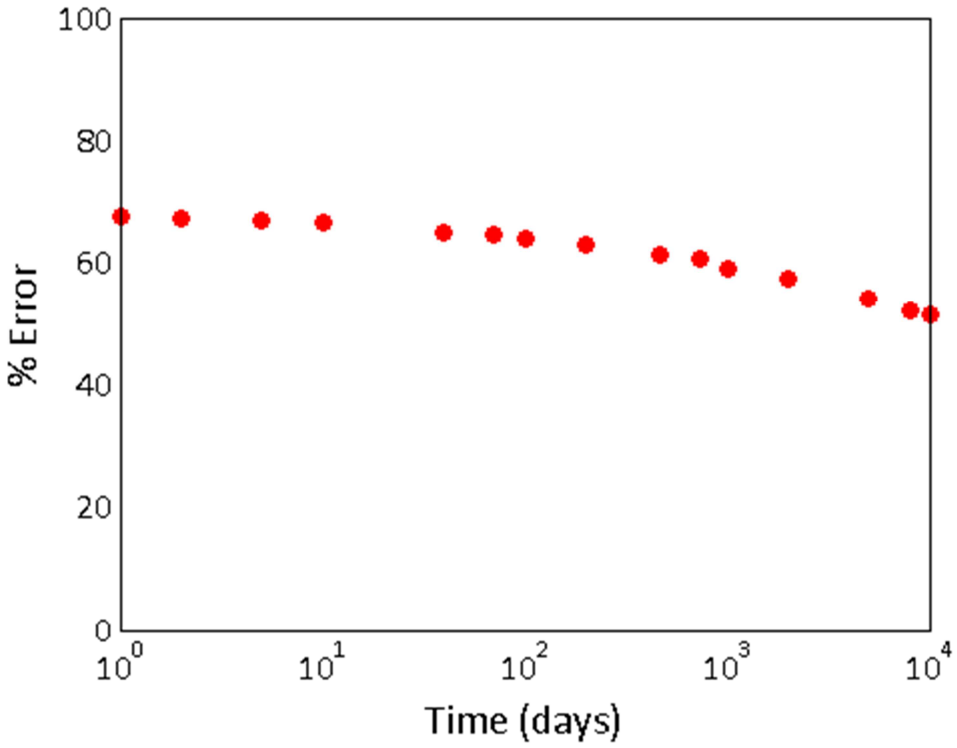


**Figure 9: Error in the heat front position due to neglecting thermal dispersion in 2-D heat transport in the plane of the fracture. Longitudinal dispersivity $\alpha_z$= 0.1 m, transverse dispersivity $\alpha_y$= 0.01 m, $2b$=100 µm, and $v$=1 m/day.**

### *Effect of Longitudinal Conduction in the Matrix on Heat Transport in the Fracture*

Figure 10 shows the 1 °C temperature contour in the numerical model domain at 250 days. The red line and the black line represent simulations with and without thermal dispersion in the fracture correspondingly. A discrete fracture with an aperture of 1000 μm is located at 15 m on the x-axis. Water flows in the fracture at a constant velocity of 50 m/day with an initial temperature of 10 °C. A point source and a 6-m line source are considered in the simulations. For the point heat source, the differences between the dispersive contour (red) and the conductive contour (black) are very evident for these conditions. The conductive simulation which neglects dispersion in the fracture underestimates the area of the thermal plume in both longitudinal and transverse directions. For the 6-m line source, the discrepancies between the dispersive and conductive solutions are observed in the vicinity of the fracture.

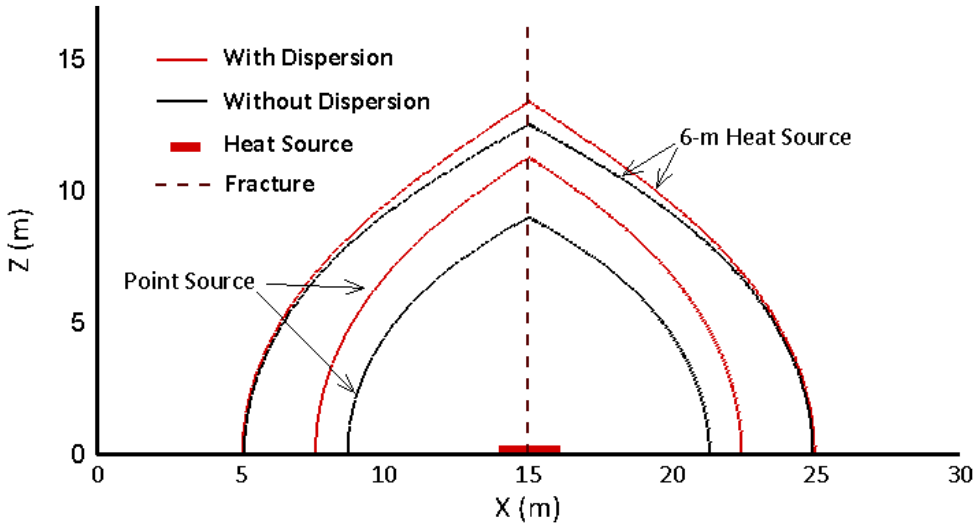


**Figure 10: The 1 °C temperature contour at 250 days obtained from the numerical model (HGS). The fracture is oriented vertically and is located x=15 m. Heat conduction is two-dimensional in the matrix. The red line and the black line represent simulations that were conducted with and without dispersion, respectively. The flow velocity equals 50 m/day, fracture aperture equals 1000 µm, and thermal dispersivity equals 1.0 m**

Figure 11 shows the temperature contours for the small aperture case at 200 days. The red line represents the dispersive contour and the black line represents the conductive contour. In this case, a discrete fracture with an aperture of 100 µm is located at 8 m on the x-axis. The flow in the fracture is constant at 10 m/day. The shapes of the contour are distinct, uniform semicircles indicating the system is completely dominated by matrix conduction. For the point source, the area of the conductive thermal plume (black) is much smaller than the area of the dispersive plume (red). In this case, neglecting dispersion in the fracture would underestimate the area of the heat plume. In contrast, dispersion is less important when the width of the line source increases to as little as 0.1-m. At the 0.1-m

source case, neglecting dispersion in the fracture causes relatively insignificant error in the temperature contour.

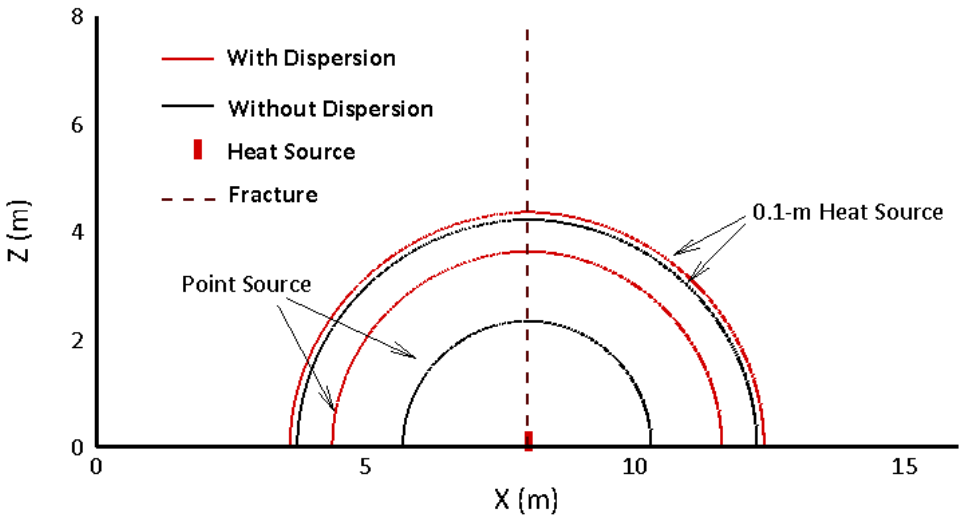


**Figure 11: The 1 °C temperature contour at 200 days obtained from the numerical model (HGS). The fracture is oriented vertically and is located x=8 m. Heat conduction is two-dimensional in the matrix. The red line and the black line represent simulations that were conducted with and without dispersion, respectively. The flow velocity equals 10 m/day, fracture aperture equals 100 µm, and thermal dispersivity equals 1.0 m**

Figure 12 shows the percentage error due to neglecting longitudinal dispersion in the fracture. The hydraulic settings are the same as used in Figure 10 in which the flow velocity is constant at 50 m/day and the fracture aperture is 1000 µm. Figure 12 shows that neglecting dispersion yields the most significant error at early time (less than one day). At the beginning of hot water injection, heat transport in the system is dominated by the transport processes (e.g. advection and dispersion) in the fracture, therefore neglecting dispersion yields large error. After 100 days of hot water injection, the system

becomes matrix conduction dominant and the transport processes in the fracture are less significant, therefore the error of neglecting longitudinal dispersion decreases to below 30%. The error for the 6-m heat source is lower than the point heat source at all times. This indicates that longitudinal dispersion in the fracture becomes less significant as the width of the heat source increases.

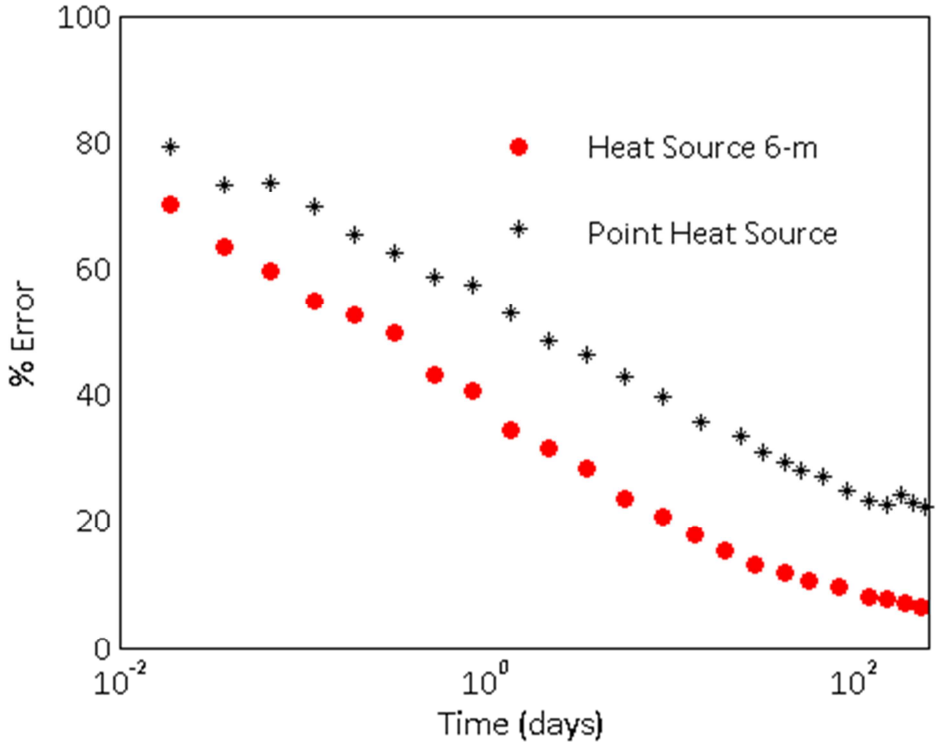


**Figure 12: Error of the heat front position due to neglecting thermal dispersion in the fracture using the numerical model (HGS). At a flow velocity of 50 m/day, an aperture of 1000 µm and thermal dispersivity (*α*) of 1.0 m.**

Figure 13 shows the percentage error due to neglecting dispersion in the fracture at flow velocity of 10 m/day and aperture of 100 µm. The conditions for these simulations are described above. The error for the 0.1-m line source is much less than the error for the point source. Neglecting dispersion causes 20% error at 0.01 day, and this error quickly

reduces to a negligible value (below 5%) after one day. At such small aperture values, conduction from the line source is the dominant transport process, therefore dispersive transport can be neglected from the fracture transport equation in this case. The percentage error data fluctuates over the range between 0.1 day and 1 day. This is due to the discretization of the model. The fluctuation has been reduced to the minimum possible by increasing the simulation time steps and refining the discretization.

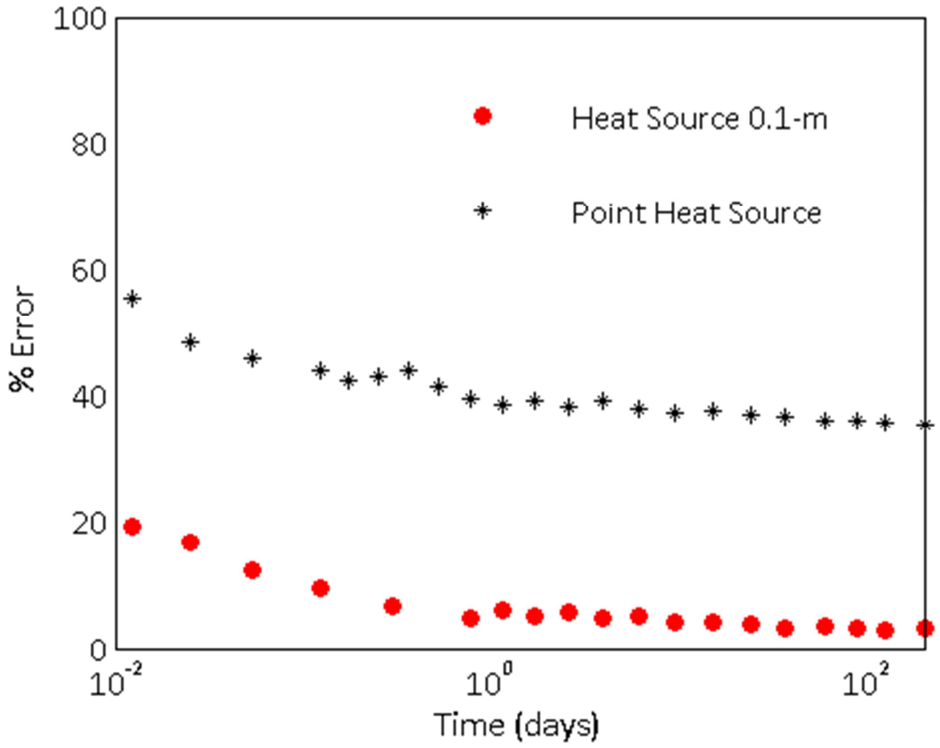


**Figure 13: Error of the heat front position due to neglecting thermal dispersion in the fracture using the numerical model (HGS), at a flow velocity of 10 m/day, an aperture of 100 µm and thermal dispersivity ($\alpha$) of 1.0 m.**

Figure 14 shows the comparison between the 1-D analytical solution and the numerical solution at an aperture of 100 μm and flow velocity of 10 m/day. For the true heat fronts , a thermal dispersivity value of 0.1 m is used in the analytical model, and a thermal dispersivity of 1.0 m is used in the numerical simulation. The percentage error for the numerical solution is about 30% less than the percentage error for the 1-D analytical results. Although a larger dispersivity is used, the effects of longitudinal dispersion are less significant in the numerical model. This suggests that the effects of longitudinal dispersion are overestimated using the 1-D analytical solutions. The reason for this overestimation is simply due to the lack of conduction in the matrix in the longitudinal direction, whereas heat can conduct in both the longitudinal and transverse directions in the numerical model. The effects of longitudinal conduction in the matrix are illustrated in Figure 4 where the location of the heat front in the fracture is significantly underestimated using the analytical solution. Comparison between the numerical and analytical solutions suggests that matrix conduction should always be considered in both directions. By including longitudinal conduction in the matrix heat transport equation, the effects of dispersion in the fracture are diminished but not eliminated. This observation agrees with the previous studies which have recently suggested that longitudinal conduction in the matrix enhances heat propagation in the longitudinal direction (Li, 2014; Ruiz Martínez et al., 2014).

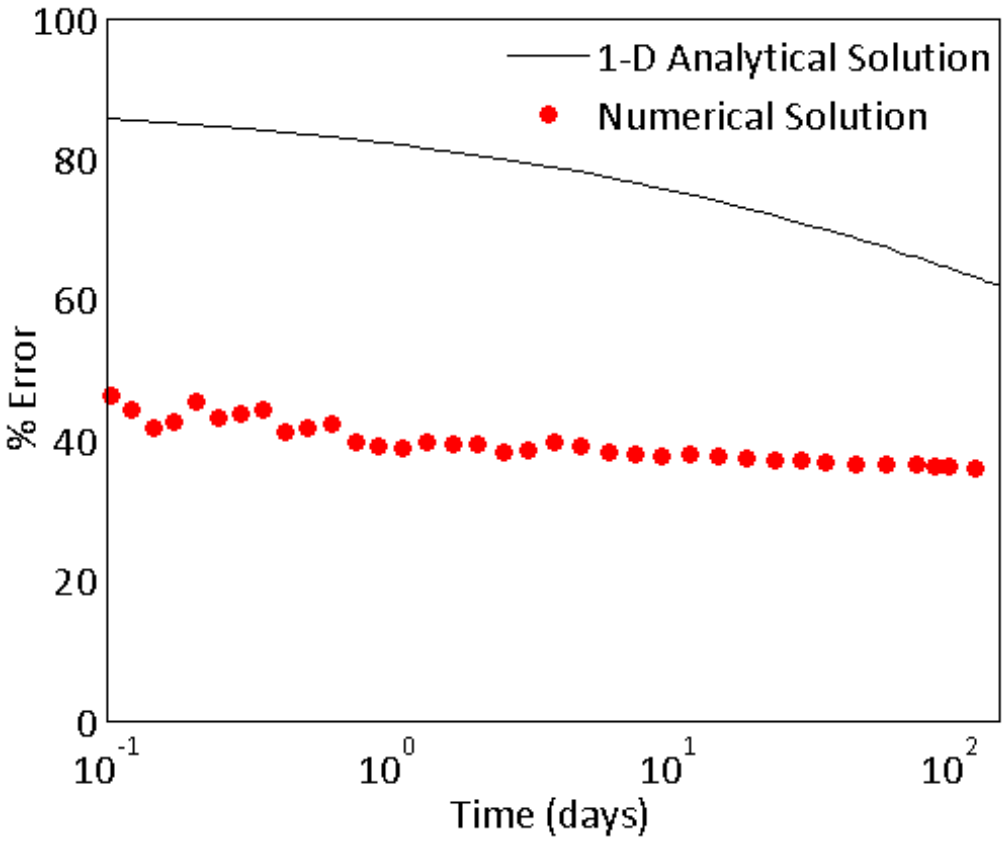


**Figure 14: Comparison between the 1-D analytical solution and the numerical solution where the thermal dispersion is neglected for both solution methods. The error is calculated at a flow velocity of 10 m/day and an aperture of 100 μm, where the true heat front is calculated in the presence of thermal dispersivity The value of thermal dispersivity ($\alpha$) equals to 0.1 m in the general solution, and it equals to 1.0 m in the numerical solution for the true heat front. The discrepancies between the results are mainly due to longitudinal conduction in the matrix.**

### 2.5 Conclusions

1-D and 2-D analytical solutions as well as numerical solutions were developed to quantify the effects of longitudinal dispersion and conduction in the fracture heat

transport equation. We assume thermal dispersion occurs through approximately the same physical processes as solute dispersion. The analytical solutions restrict matrix conduction in the direction perpendicular to the fracture, whereas the numerical solution considers it in both longitudinal and transverse directions. A large and a small fracture aperture are selected to study the percentage error that results from neglecting these processes. Several conclusions can be drawn from this study:

1. Longitudinal thermal conduction and dispersion in the fracture are critical processes that affect heat propagation in fractured rock environment, especially at small apertures, high flow rate and the beginning of hot water injection.
2. Transverse thermal dispersion in the fracture plane is observed to be an important transport process leading to retardation of the migrating heat front particularly after 40 days of hot water injection.
3. The width of the heat source is an important parameter that significantly influences the heat transport in the system. More specifically, the effects of thermal dispersion in the fracture are observed to decrease when the width of the heat source expands.
4. Longitudinal conduction in the matrix is clearly the most important process that determines temperature distribution in the system for most conditions. The longitudinal conduction in the matrix decreases the effects of dispersion in the fracture.

## 2.6 Literature Cited


Unger, A., Sudicky, E.A., 1991. Solute Transport in a Single Horizontal Fracture Situated in a Porous Rock Matrix. Department of Earth Sciences, University of Waterloo. Unpublished report.

Audouin, O., Bodin, J., 2008. Cross-borehole slug test analysis in a fractured limestone aquifer. Journal of Hydrology 348, 510–523.

Bader, S., Kooi, H., 2005. Modelling of solute and water transport in semi-permeable clay membranes: Comparison with experiments. Advances in Water Resources 28, 203–214.

Bagalkot, N., Kumar, G.S., 2014. Thermal front propagation in variable aperture fracture – matrix system : A numerical study. Sadhana 40, 605–622.

Baston, D.P., Kueper, B.H., 2009. Thermal conductive heating in fractured bedrock: Screening calculations to assess the effect of groundwater influx. Advances in Water Resources 32, 231–238.

Berkowitz, B., 2002. Characterizing flow and transport in fractured geological media: A review. Advances in Water Resources 25, 861–884.

Bodin, J., Delay, F., de Marsily, G., 2003. Solute transport in a single fracture with negligible matrix permeability: 1. fundamental mechanisms. Hydrogeology Journal 11, 418–433.

Bödvarsson, G.S., Tsang, C.F., 1982. Injection and Thermal Breakthrough in Fractured Geothermal Reservoirs. Journal of Geophysical Research 87, 1031–1048.

Cheng, A.H.-D., Ghassemi, A., Detournay, E., 2001. Integral equation solution of heat extraction from a fracture in hot dry rock. International Journal for Numerical and Analytical Methods in Geomechanics 25, 1327–1338.

Côté, J., Grosjean, V., Konrad M., J., 2012. Thermal conductivity of bitumen concrete. Canadian Journal of Civil Engineering 40, 172–180.

de Hoog, F.R., Knight, J.H., Stokes, a. N., 1982. An Improved Method for Numerical Inversion of Laplace Transforms. SIAM Journal on Scientific and Statistical Computing 3, 357–366.

de Marsily, G., 1986. Quantitative Hydrogeology: Groundwater Hydrology for Engineers. Academic, Orlando,Florida.

Doe, T., Mclaren, R., Dershowitz, W., 2014. Discrete Fracture Network Simulations of Enhanced Geothermal Systems, in: 39th Workshop on Geothermal Reservoir Engineering. Stanford.

Ferguson, G., 2007. Heterogeneity and Thermal Modeling of Ground Water. Groundwater 45, 185–490.

Gan, Q., Elsworth, D., 2014. Thermal drawdown and late-stage seismic-slip fault reactivation in enhanced geothermal reservoirs. Journal of Geophysical Research 1–14.

Ganguly, S., Kumar, M.S.M., 2014. Analytical solutions for transient temperature distribution in a geothermal reservoir due to cold water injection. Hydrogeology Journal 22, 351–369.

Gelhar, L.W., Welty, C., Rehfeldt, K.R., 1992. A critical review of data on field-scale dispersion in aquifers. Water Resources Research 28, 1955–1974.

Ghassemi, A., Zhou, X., 2011. A three-dimensional thermo-poroelastic model for fracture response to injection/extraction in enhanced geothermal systems. Geothermics 40, 39–49.

Gringarten, A.C., Witherspoon, P.A., Ohnishi, Y., 1975. Theory of heat extraction from fractured hot dry rock. Journal of Geophysical Research 80, 1120–1124.

Guimera, J., Carrera, J., 2000. A comparison of hydraulic and transport parameters measured in low-permeability fractured media. Journal of Contaminant Hydrology 41, 261–281.

Guo, R., 2015. Thermal Modelling of a Mark II Container. Toronto, Canada.

Hollenbeck, K.J., 1998. INVLAP.M: A matlab function for numerical inversion of Laplace transforms by the de Hoog algorithm.

Jung, Y., Pruess, K., 2012. A closed-form analytical solution for thermal single-well injection-withdrawal tests. Water Resources Research 47.

Klepikova, M. V., Le Borgne, T., Bour, O., Gallagher, K., Hochreutener, R., Lavenant, N., 2014. Passive temperature tomography experiments to characterize transmissivity and connectivity of preferential flow paths in fractured media. Journal of Hydrology 512, 549–562.

Lapcevic, P.A., Novakowski, K.S., Sudicky, E.A., 1999. The interpretation of a tracer experiment conducted in a single fracture under conditions of natural groundwater flow. Water Resources Research 35, 2301–2312.

Li, W., 2014. Numerical and Analytical Modeling of Heat Transfer between Fluid and Fractured Rocks. Massachusetts Institute of Technology.

Lu, W., Xiang, Y., 2012. Experiments and sensitivity analyses for heat transfer in a meter-scale regularly fractured granite model with water flow. Journal of Zhejiang University -SCIENCE A 13, 958–968.

Metzger, T., Didierjean, S., Maillet, D., 2004. Optimal experimental estimation of thermal dispersion coefficients in porous media. International Journal of Heat and Mass Transfer 47, 3341–3353.

Molina-Giraldo, N., Bayer, P., Blum, P., 2011. Evaluating the influence of thermal dispersion on temperature plumes from geothermal systems using analytical solutions. International Journal of Thermal Sciences 50, 1223–1231.

Neuman, S.P., 2005. Trends, prospects and challenges in quantifying flow and transport through fractured rocks. Hydrogeology Journal 13, 124–147.

Novakowski, K., Bickerton, G., Lapcevic, P., Voralek, J., Ross, N., 2006. Measurements

of groundwater velocity in discrete rock fractures. Journal of Contaminant Hydrology 82, 44–60.

Novakowski, K., Evans, G., Lever, D., Raven, K., 1985. A field example of measuring hydrodynamic dispersion in a single fracture. Water Resources Research 21, 1165–1174.

Oron, A.P., Berkowitz, B., 1998. Flow in rock fractures: The local cubic law assumption reexamined. Water Resources Research 34, 2811.

Özisik, M.N., 1980. Heat Conduction. John Wiley & Sons, 605 Third Avenue, New York.

Rau, G.C., Andersen, M.S., Acworth, I.R., 2012. Experimental investigation of the thermal dispersivity term and its significance in the heat transport equation for flow in sediments. Water Resources Research 48.

Raymond, J., Therrien, R., 2014. Optimizing the design of a geothermal district heating and cooling system located at a flooded mine in Canada. Hydrogeology Journal 22, 217–231.

Ruiz Martínez, Á., Roubinet, D., Tartakovsky, D.M., 2014. Analytical models of heat conduction in fractured rocks. Journal of Geophysical Research 119, 83–98.

Saar, M.O., 2011. Review: Geothermal heat as a tracer of large-scale groundwater flow and as a means to determine permeability fields. Hydrogeology Journal 19, 31–52.

Sauty, J.P., Gringarten, A.C., Fabris, H., Thiery, D., Menjoz, A., Landel, P.A., 1982a. Sensible energy storage in aquifers: 2. Field experiments and comparison with theoretical results. Water Resources Research 18, 253–265.

Sauty, J.P., Gringarten, A.C., Menjoz, A., Landel, P.A., 1982b. Sensible energy storage in aquifers: 1. Theoretical study. Water Resources Research 18, 245.

Simms, R.B., Haslam, S.R., Craig, J.R., 2014. Impact of soil heterogeneity on the functioning of horizontal ground heat exchangers. Geothermics 50, 35–43.

Tang, D.H., Frind, E.O., Sudicky, E.A., 1981. Contaminant transport in fractured porous media: Analytical solution for a single fracture. Water Resources Research 17, 555–564.

Therrien, R., McLaren, R.G., Sudicky, E.A., Panday, S., 2010. HydroGeoSphere: A three-domentional numerical model describing fully-integrated subsurface and surface flow and solute transport. Québec.

Wang, Q., Zhan, H., 2015. On different numerical inverse laplace methods for solute transport problems. Advances in Water Resources 75, 80–92.

West, M.R., Kueper, B.H., Novakowski, K.S., 2004. Semi-analytical solutions for solute transport in fractured porous media using a strip source of finite width. Advances in Water Resources 27, 1045–1059.

Wu, B., Zhang, X., Jeffrey, R.G., Bunger, A.P., Huddlestone-Holmes, C., 2015. Perturbation analysis for predicting the temperatures of water flowing through multiple parallel fractures in a rock mass. International Journal of Rock Mechanics

and Mining Sciences 76, 162–173.

Yang, J., Latychev, K., Edwards, R.N., 1998. Numerical computation of hydrothermal fluid circulation in fractured Earth structures. Geophysical Journal International 135, 627–649.

Yang, S.Y., Yeh, H.D., 2009. Modeling heat extraction from hot dry rock in a multi-well system. Applied Thermal Engineering 29, 1676–1681.

Yoshida, K., Shimizu, A., Fomin, S., Hashida, T., 2003. Computer simulation of fluid flow in fractured media. Effect of thermal dispersion, in: Sixth International Workshop on Nondestructive Testing and Computer Simulations in Science and Engineering. pp. 207–215.

Zeng, Y.C., Wu, N.Y., Su, Z., Wang, X.X., Hu, J., 2013. Numerical simulation of heat production potential from hot dry rock by water circulating through a novel single vertical fracture at Desert Peak geothermal field. Energy 63, 268–282.

Zhou, Q., Liu, H.H., Molz, F.J., Zhang, Y., Bodvarsson, G.S., 2007. Field-scale effective matrix diffusion coefficient for fractured rock: results from literature survey. Journal of Contaminant Hydrology 73, 161–187.

# Chapter 3

## Conclusions and Recommendations

The objective of this study was to examine the effects of longitudinal conduction and dispersion for heat transport in a discrete fracture embedded in a rock matrix of low permeability. To achieve this objective, 1-D and 2-D analytical solutions as well as numerical analysis were developed to explore heat transport in fractured rock environments with and without dispersion and conduction. This was carried out for two source conditions, the first in which the source is located as a discrete point or plane in the fracture and the second in which the source is distributed across the fracture origin and the surrounding matrix. Several conclusions can be drawn from this study:

1. Longitudinal thermal conduction and dispersion in the fracture are critical processes that affect heat propagation in fractured rock environments, especially at small apertures, high flow rate and the beginning of hot water injection.
2. Transverse dispersion in the fracture plane is also an important transport process. Solutions which neglect dispersion in the transverse direction underestimate the location of heat fronts in the first five days and overestimate after 40 days of hot water injection.
3. The width of the heat source is an important parameter that determines heat transport in the system. The effects of dispersion can be decreased by expanding the width of the heat sources.
4. Longitudinal conduction in the matrix is an important process that determines temperature distribution in the system and decreases the effects of dispersion in the fracture.

Through this fundamental study, areas requiring further research became apparent. While numerous analytical and numerical models have been developed to study the transport of heat in fractured rock environments, more laboratory-scale and field-scale experiments are required to verify these models. For example, measurement of the thermal dispersivity value in a single fracture would help us to better understand thermal dispersion and how it differs from solute dispersion.

This study further supports the suggestion that conduction in the matrix is an important process that determines the temperature distribution in a fractured porous medium, especially at time-to-equilibrium. Future research will focus on the processes and parameters that could affect heat transport in the matrix. For example, the heterogeneity of the matrix conductivity of the host rock could have impacts on the temperature distribution in a geothermal reservoir.

In this study, 2-D dispersive transport in the fracture and 2-D conductive transport in the matrix were separately studied, using a 2-D analytical model and a numerical model, respectively. There is clearly a need to develop an analytical model that incorporates 2-D transport processes in both the fracture and the matrix. This model could be used to study more extensively the effects on dispersive transport in the fracture plane due to 2-D conduction in the matrix.

Through the analyses using the numerical model, the heat front location is defined as the location in the fracture at where temperature equals to 1 ˚C. For future study, it is

recommended to define the front at a lower temperature (e.g. 0.01 ˚C). A lower definition of the front temperature is important for measuring the thermal dispersivity. This is a practical problem that presently limits our ability to analyze the detection of heat breakthrough through fractures between wells.

## Appendix A 2-D Analytical Solution Development

The one dimensional differential transport equation for the porous matrix can be written as:

$$\frac{\partial T'}{\partial t} - \frac{\lambda_m}{c_m \rho_m} \frac{\partial^2 T'}{\partial x^2} = 0 \qquad (A1)$$

The boundary conditions and initial conditions for eq. (A1) are

$$T'(x, y, z, 0) = 0 \qquad (A2)$$

$$T'(b, y, z, t) = T(b, y, z, t) \qquad (A3)$$

$$T'(\infty, y, z, t) = 0 \qquad (A3)$$

From Yang et al. (1998), the solution to eq. (A1) in Laplace space is given as:

$$\bar{T}' = \bar{T} \exp[-\left(\frac{c_m \rho_m}{\lambda_m} s\right)^{\frac{1}{2}} (x - b)\,] \qquad (A4)$$

The gradient of $\bar{T}'$ at the interface $x=b$ is:

$$\left.\frac{d\bar{T}'}{dt}\right|_{x=b} = -\bar{T}\left(\frac{c_m \rho_m}{\lambda_m} s\right)^{\frac{1}{2}} \qquad (A5)$$

The 2-D differential equation for the fracture can be written as:

$$\frac{\partial T}{\partial t} + v\frac{\partial T}{\partial z} - \frac{\lambda_m}{c_w \rho_w}\frac{\partial^2 T}{\partial z^2} - \frac{\lambda_m}{c_w \rho_w}\frac{\partial^2 T}{\partial x^2} - \left.\frac{\lambda_m}{c_w \rho_w b}\frac{\partial T'}{\partial x}\right|_{x=b} = 0 \qquad (A6)$$

The boundary conditions and initial conditions for eq. (A6) are

$$T(x, y, z, 0) = 0 \tag{A7}$$

$$T(x, y, \infty, t) = 0 \tag{A8}$$

$$T(x, y, 0, t) = T_0 \delta(y - y') \tag{A9}$$

$$\frac{\partial T}{\partial y}(x, 0, z, t) = 0 \tag{A10}$$

$$\frac{\partial T}{\partial y}(x, H, z, t) = 0 \tag{A11}$$

The Laplace transform is applied to eq. (A6) followed by substitution of eq. (A5) to yield:

$$\frac{\partial^2 \bar{T}}{\partial z^2} + \frac{\partial^2 \bar{T}}{\partial y^2} - \frac{V}{\eta}\frac{\partial \bar{T}}{\partial z} - \frac{1}{\eta}\left(s + \frac{S^{\frac{1}{2}}}{A}\right)\bar{T} = 0 \tag{A12}$$

Applying the finite cosine Fourier transform to eq. (A12) and rearranging gives:

$$\frac{d^2 \hat{T}}{dz^2} - \frac{V}{\eta}\frac{d\hat{T}}{dz} - \left[\frac{n^2\pi^2}{H^2} + \frac{1}{\eta}\left(s + \frac{s^{\frac{1}{2}}}{A}\right)\right]\hat{T} = 0 \tag{A13}$$

Eq. (10) is a second-order ordinary differential equation which has a solution of the form

$$\hat{T}(x, n, z, p) = A\, EXP\left(r_{(+)}z\right) + B\, EXP\left(r_{(-)}z\right) \tag{A14}$$

where A and B are undetermined constant, and r is given as:

$$r = \frac{v}{2\eta} \mp \left[\frac{v^2}{4\eta^2} + \frac{n^2\pi^2}{H^2} + \frac{1}{\eta}\left(s + \frac{s^{\frac{1}{2}}}{A}\right)\right]^{1/2} \tag{A15}$$

Applying transformed boundary condition eq. (A8), the first term in eq. (A14) must vanish. Then, substituting transformed eq. (A9), we found:

$$B = \frac{T_0}{s}\cos\left(\frac{n\pi y'}{H}\right) \tag{A16}$$

Then the solution of eq.(10) in Fourier and Laplace space is:

$$\hat{T}(x,n,z,p) = \frac{T_0}{s}\cos\left(\frac{n\pi y'}{H}\right) exp\left(\frac{vz}{2\eta}\right)$$

$$\times exp\left\{-z\left[\frac{v^2}{4\eta^2} + \frac{n^2\pi^2}{H^2} + \frac{1}{\eta}\left(s + \frac{s^{\frac{1}{2}}}{A}\right)\right]^{1/2}\right\} \tag{A17}$$

Applying the inverse finite cosine Fourier transform to eq. (A17) yields:

$$\bar{T}(x,y,z,s)$$

$$= \frac{T_0}{Hs} exp\left(\frac{vz}{2\eta}\right) \times exp\left\{-z\left[\frac{v^2}{4\eta^2} + \frac{1}{\eta}\left(s + \frac{s^{\frac{1}{2}}}{A}\right)\right]^{1/2}\right\}$$

$$+ \frac{2}{H}\sum_{n=1}^{\infty}\frac{T_0}{s}\cos\left(\frac{n\pi y'}{H}\right) exp\left(\frac{vz}{2\eta}\right) \times exp\left\{-z\left[\frac{v^2}{4\eta^2} + \frac{n^2\pi^2}{H^2} + \frac{1}{\eta}\left(s + \frac{s^{\frac{1}{2}}}{A}\right)\right]^{1/2}\right\}$$

$$\times \cos\left(\frac{n\pi y}{H}\right) \tag{A18}$$

To obtain the line source, integral operation is required over the length of the heat source.

$$\bar{T}(x,y,z,s) = \int_{D_1}^{D_1+2B} \bar{T}\,(x,y,z,s)dy' \qquad (A19)$$

Integrating eq. (A18) with respect to the source geometry gives the final solution:

$$\bar{T}(x,y,z,s) = \frac{2BT_0}{Hs} exp\left(\frac{vz}{2\eta}\right) \times exp\left\{-z\left[\frac{v^2}{4\eta^2} + \frac{1}{\eta}\left(s + \frac{s^{\frac{1}{2}}}{A}\right)\right]^{\frac{1}{2}}\right\} + \frac{2T_0}{s} exp\left(\frac{vz}{2\eta}\right)$$

$$\times \sum_{n=1}^{\infty} \frac{1}{n\pi} \cos\left(\frac{n\pi y}{H}\right) \times \left[\sin\frac{n\pi(D_1+2B)}{H} - \sin\frac{n\pi D_1}{H}\right]$$

$$\times exp\left\{-z\left[\frac{v^2}{4\eta^2} + \frac{n^2\pi^2}{H^2} + \frac{1}{\eta}\left(s + \frac{s^{\frac{1}{2}}}{A}\right)\right]^{\frac{1}{2}}\right\} \qquad (A19)$$

## Appendix B Numerical Model Verification

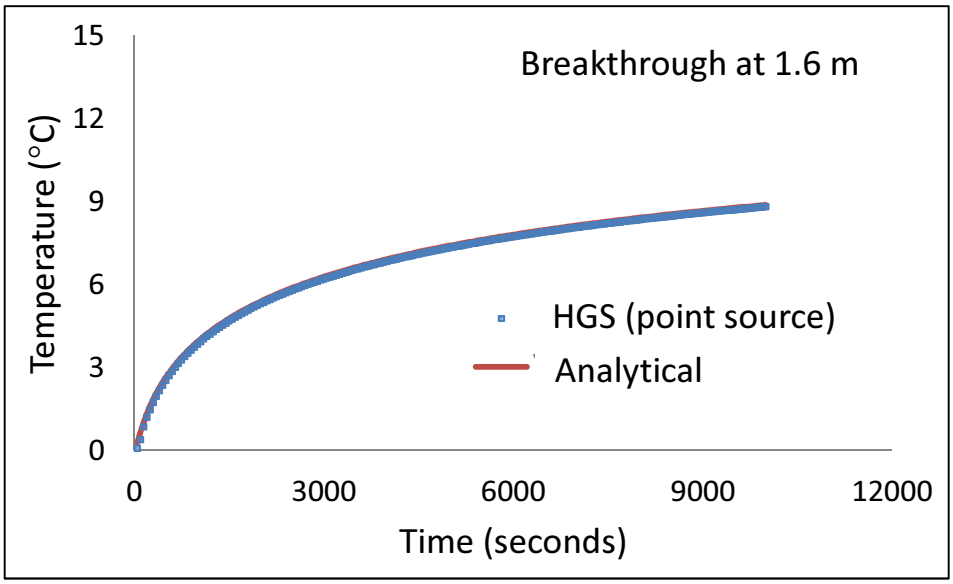


(a)

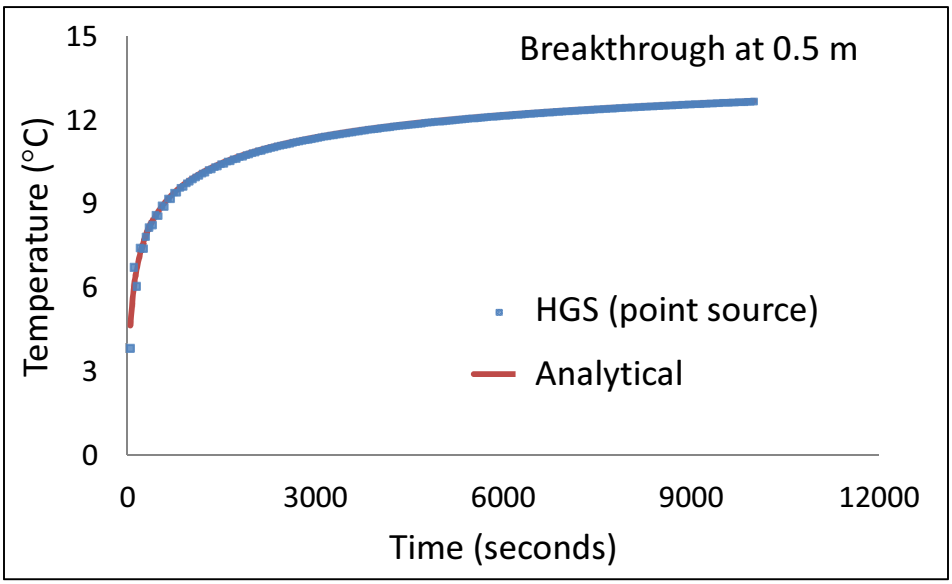


(b)

**Figure A. 1 Comparison between the temperature breakthrough results from the analytical solution and HGS. At aperture, 2b= 300 um, and flow velocity 0.05 m/s, the two solutions show strong agreement (note that the two curves overlap each other). This indicates the effects of longitudinal matrix conduction are insignificant at the extreme flow condition.**

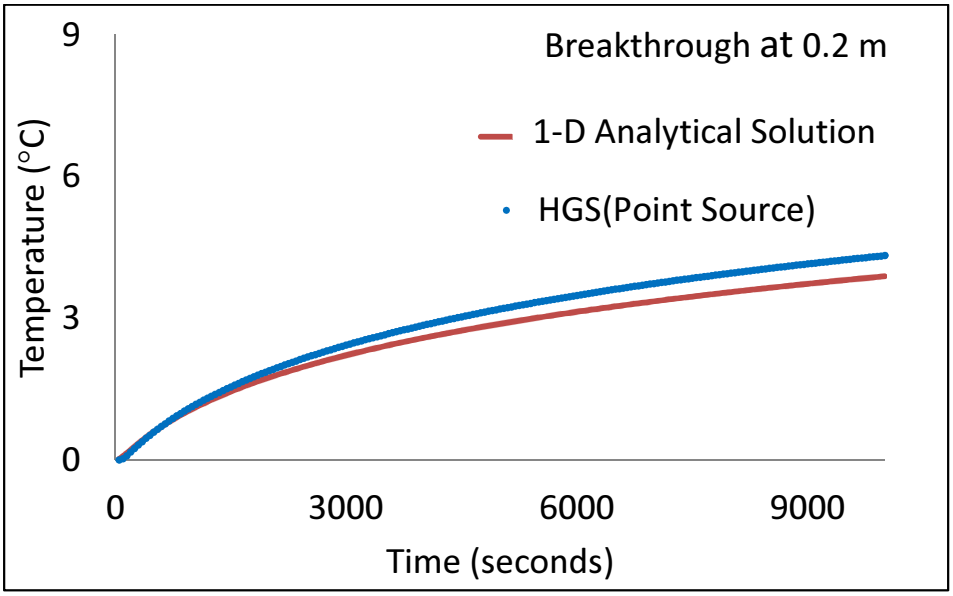


(a)

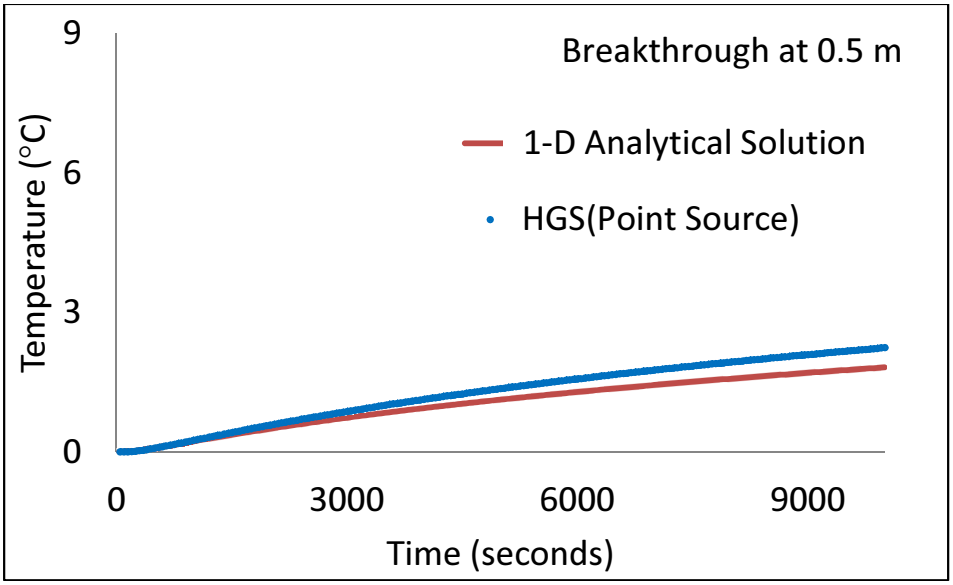


(b)

**Figure A. 2 Comparison between the temperature breakthrough results from the analytical solution and HGS. At aperture, 2b= 300 um, and flow velocity 0.0005 m/s, temperature differences are observed between the analytical solution and HGS due to the inclusion of 2-D conduction in the matrix in the numerical model..**

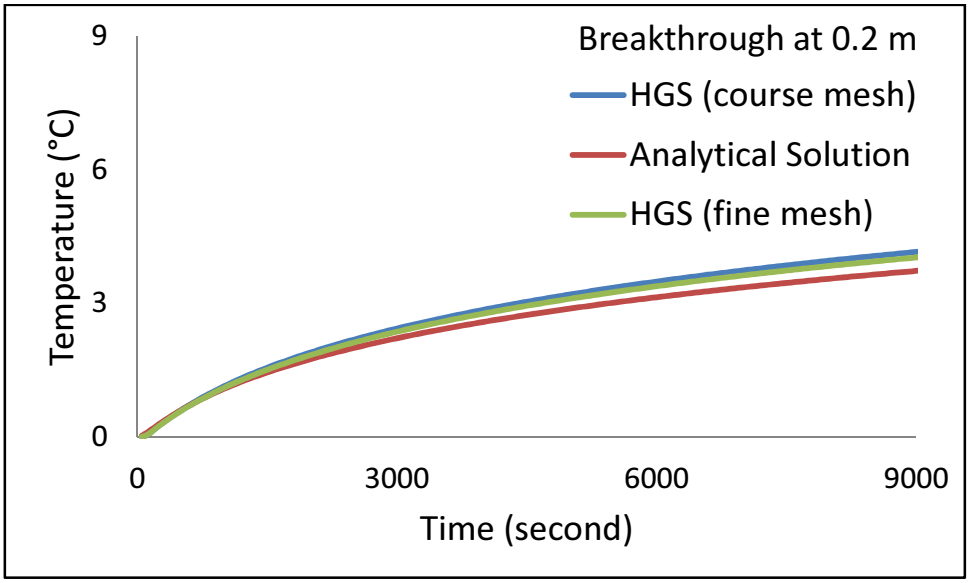


(a)

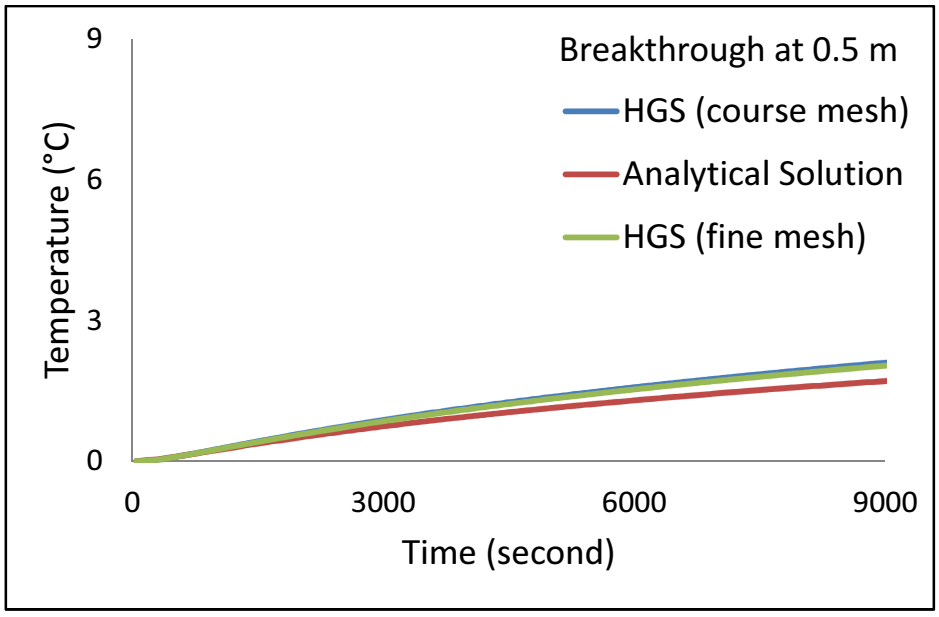


(b)

**Figure A. 3 The mesh in the numerical model is refined to study the effects of discretization. At a finer mesh, discrepancies between the analytical and numerical models are still observed. This indicates the differences between the two solutions are not influenced by the discretization.**

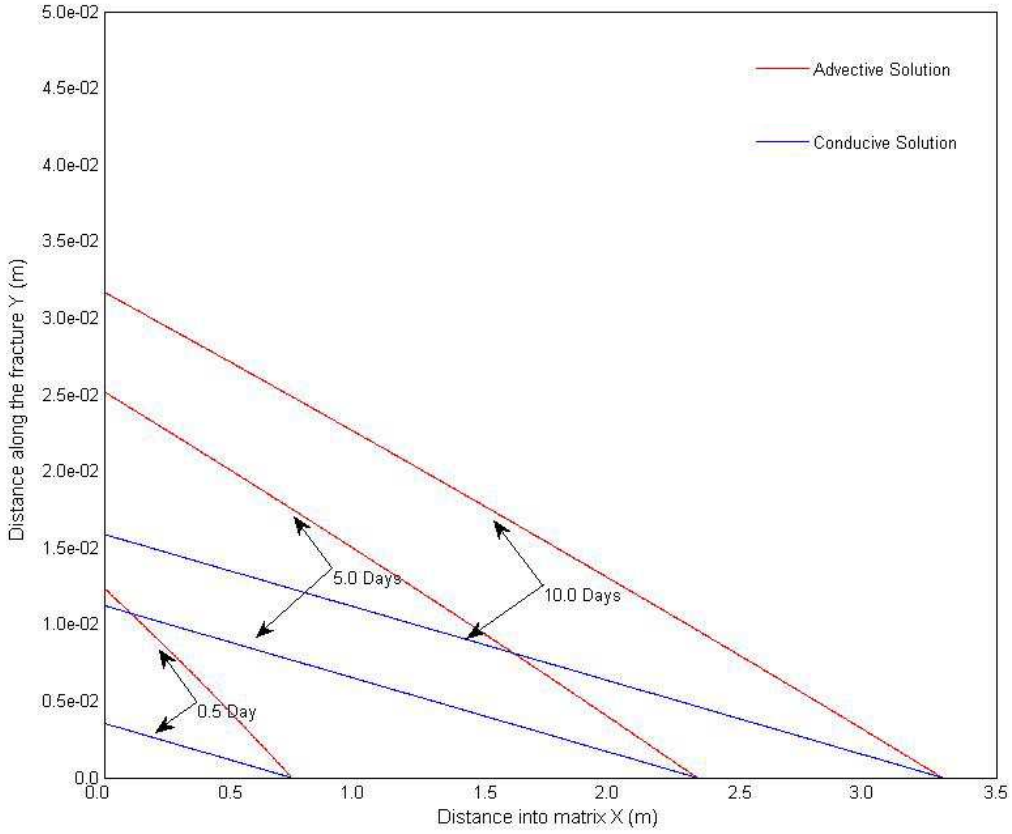


**Figure A. 4 Comparison between longitudinal conduction in the fracture (red) versus pure advection (blue) for a 0.01 °C temperature contour in the domain, aperture, 2b =200 µm and flow velocity, v = 2 m/day. The heat penetration in the matrix is one magnitude deeper than the fracture. This suggests that the analytical solutions underestimate the temperature in the fracture. The underestimation of the heat front in the fracture is due to the simplification made in the matrix equation which restricts conduction in the horizontal direction.**

## Appendix C Sample HydroGeoSphere Input Code

**Grok File**

```
numerical solution for heat transport in a single fracture
point source, 2b=1000um, v=50m/day, dispersivity=1m
end title

!_____________________________ grid definition
generate blocks interactive
grade x
15.0 0.0 0.01 1.1 0.2
grade x
15.0 30.0 0.01 1.1 0.2
grade y
0.0 2.0 1.0 1.0 1.0
grade z
0.0 20.0 0.01 1.1 0.05
grade z
20.0 30.0 0.05 1.1 0.1
end
end

!_____________________________ porous media properties
use zone type
porous media
properties file
meyer.mprops
clear chosen zones
choose zones all
read properties
porous medium

!_____________________________ heat transfer parameters
do heat transfer
thermal conductivity of bulk
2.0
specific heat capacity of solid
800
solid density
2650

specific heat capacity of water
4174
thermal conductivity of water
0.5
mechanical heat dispersion
```

```
end heat transfer
fluid density
997.0d0
fluid viscosity
1.3d-3
solute
name
temperature
temperature species
end solute

!_____ solver parameters
units: kilogram-metre-second
echo to output

!---------- Timestep controls

initial time
50.0d0
initial timestep
1000.0d0
concentration control
0.5d0

output times
2592000.0d0
8640000.0d0
17280000.0d0
25920000.0d0
end

!_____ initial conditions for flow
clear chosen nodes
choose nodes all
initial head
0.0000001d0

!_____ boundary conditions for flow
!left boundary
clear chosen nodes
choose nodes z plane
0.0
0.001
specified head
1.0
0.0 0.0276d0
```

```
!right boundary
clear chosen nodes
choose nodes z plane
30.0
0.001
specified head
1
0.0 0.00001d0

!_____ initial conditions for heat transfer
clear chosen nodes
choose nodes all
initial concentration
0

!_____ boundary conditions for heat transfer

!lower boundary
clear chosen nodes
choose nodes block
15.0d0 15.0d0
0.0d0 2.0d0
0.0d0 0.0d0
specified concentration
1                ! number of time panels
0.0 1.0d20 10.0      ! timeon. time off. species 1. 2. 3 concentration

!_____ fracture media properties

use zone type
fracture
properties file
meyer.fprops
clear chosen faces
choose faces x plane
15.0d0
1.0d-9
new zone
1
clear chosen zones
choose zone number
1
read properties
fracture1

!_____ geometry output
```

make observation point
obs_f
15.0 1.0 1.0
make observation point
obs_f2
15.0 1.0 2.0
make observation point
obs_f3
15.0 1.0 3.0
make observation point
obs_bc
0.1 1.0 0.1
make observation well
obs_well_fracture
15.0 0.0 0.0
15.0 0.0 14.0

**Fprops File**

fracture1
aperture
1000.0d-6
longitudinal dispersivity
1.0

transverse dispersivity
4.0d0
end

**Mprops File**

!----------
porous medium

k isotropic
1.e-50

porosity
0.002

longitudinal dispersivity
1d-3

transverse dispersivity

1d-3

vertical transverse dispersivity
1d-3

tortuosity
1.0

end material
!----------

## Appendix D Sample Matlab Code for Analytical Solutions

### 1-D General Solution

```
function [x,Tf ] = Yangetal( v,b,t,z )
km= 2;  %thermal conductivity of matrix
kw= 0.5; %thermal conductivity of water
cm= 800; % Heat capacity of matrix
pm=2650; % density of matrix
pw=1000; %density of water
cw=4174; %specific heat of water
%v=0.005; %flowrate
%b= 0.0005; %half of the fracture aperture
A=b*cw*pw/sqrt(km * cm * pm);
X = kw/(cw*pw); %Variable X
beta = 4*X/v^2; %Variable Beta Square
y=v/(2*X); %Variable y
To=10; %Initial Temperature
alpha=0; % default for largest pole for function
tol=1e-9;

for i = 1:length(z)
T(i)=invlap('yangfracture',t,alpha,tol,y,z(i),beta,A,To );
end

x=linspace(b,10,10);
clearvars i

for i=1:length(z)
   for j = 1:length(x) %horizontal
   Tp(i,j)=To .* invlap('yangmatrix',t,alpha,tol,cm,pm,km,b,x(j),y,z(i),beta,A );
     end
end

Tf= horzcat(T',Tp); %combine fracture and matrix together
```

```
x = horzcat(0,x);
end

function [ F ] = yangfracture( s,y,z,beta,A,To )
 F= To./s.*exp(z*y-z*y.*sqrt(1+ beta.*(s + s.^0.5./A)));
end

function [ Fp ] = yangmatrix( s,cm,pm,km,b,x,y,z,beta,A )
Fp = 1./s.*exp(z*y-z*y.*sqrt(1+ beta.*(s + s.^0.5./A))...
    -sqrt( cm * pm .* s./km) .* (x-b));

end
```

**2-D General Solution**

```
function [ GT ] = TWODFracGeneral( velocity,Aperture,z,y,t,n,H,B)
v=velocity/86400; %m/s
b= Aperture*1e-6; %half of the aperture m
alpha=0; % default for largest pole for function
tol=1e-9;
    Tsum2=invlap('SummationTerm',t,alpha,tol,y,z,B,v,n,H,b)
    Tf=invlap('TWODFirstTerm',t,alpha,tol,H,z,B,v,b);
GT=Tf+Tsum2;
end

function [ Ts ] = SummationTerm( s,y,z,B,v,m,H,b)
km= 2;  %thermal conductivity of matrix
cm= 800; % Heat capacity of matrix
pm=2650; % density of matrix
pw=1000; %density of water
cw=4174; %specific heat of water
kz= 0.5+0.1*v*pw*cw; %effective thermal conductivity in the flow direction
```

```
ky=0.5+0.01*v*pw*cw; % transverse effective thermal conductivity
A=b*cw*pw/sqrt(km * cm * pm);
X = kz/(cw*pw); %Variable X
D1=H/2-B;
To=1;
p=s;
T=zeros(1,length(m));
Ts=zeros(length(p),1);
for i=1:length(p)
   s=p(i);
   for j=1:length(m)
      n=m(j);
T(j)=  2*To./s.*...
   1/(n*pi)*cos(n*pi*y/H)*...
    (sin(n*pi*(D1+2*B)/H)-sin(n*pi*D1/H)).*...
    exp(v*z/(2*X)-z*sqrt(v^2/(4*X^2)+ky/kz*n^2*pi^2/H^2 +1/X.*(s+s.^0.5./A)));
   end
   Ts(i,:)=sum(T);
end
end

function [ F ] = TWODFirstTerm( s,H,z,B,v,b )
km= 2;  %thermal conductivity of matrix
cm= 800; % Heat capacity of matrix
pm=2650; % density of matrix
pw=1000; %density of water
cw=4174; %specific heat of water
kz= 0.5+2*v*pw*cw; %effective thermal conductivity in the flow direction
ky= 0.5+0.2*v*pw*cw; % transverse effective thermal conductivity
A=b*cw*pw/sqrt(km * cm * pm);
X = kz/(cw*pw); %Variable X
D1=H/2-B;
To=1;
F= 2*B*To./H.*s.*...
```

```
    exp( v*z/(2*X)-z.*sqrt(v^2/(4*X^2) + 1/X.*(s+sqrt(s)./A)));
end
```

**2-D Conductive Solution**

```
function [ GT ] = TWODFracNodis( velocity,Aperture,z,y,t,n,H,B)
v=velocity/86400; %m/s
b= Aperture*1e-6; %half of the aperture m
alpha=0; % default for largest pole for function
tol=1e-9;
   Tsum2=invlap('NodisSummationTerm',t,alpha,tol,y,z,B,v,n,H,b);
   Tf=invlap('NodisFirstTerm',t,alpha,tol,H,z,B,v,b);
GT=Tf+Tsum2;
end

function [ F ] = NodisFirstTerm( s,H,z,B,v,b )
km= 2;  %thermal conductivity of matrix
kw= 0.5; %effective thermal conductivity in the flow direction
cm= 800; % Heat capacity of matrix
pm=2650; % density of matrix
pw=1000; %density of water
cw=4174; %specific heat of water
A=b*cw*pw/sqrt(km * cm * pm);
X = kw/(cw*pw); %Variable X
D1=H/2-B;
To=1;
F= 2*B*To./H.*s.*...
    exp( v*z/(2*X)-z.*sqrt(v^2/(4*X^2) + 1/X.*(s+sqrt(s)./A)));
end

function [ Ts ] = NodisSummationTerm( s,y,z,B,v,m,H,b)
km= 2;  %thermal conductivity of matrix
kw=0.5; %effective thermal conductivity in the flow direction
```

```
cm= 800; % Heat capacity of matrix
pm=2650; % density of matrix
pw=1000; %density of water
cw=4174; %specific heat of water
A=b*cw*pw/sqrt(km * cm * pm);
X = kw/(cw*pw); %Variable X
D1=H/2-B;
To=1;
p=s;
T=zeros(1,length(m));
Ts=zeros(length(p),1);
for i=1:length(p)
   s=p(i);
      for j=1:length(m)
         n=m(j);
T(j)=  2*To./s.*...
   1/(n*pi)*cos(n*pi*y/H)*...
    (sin(n*pi*(D1+2*B)/H)-sin(n*pi*D1/H)).*...
    exp(v*z/(2*X)-z*sqrt(v^2/(4*X^2)+n^2*pi^2/H^2 +1/X.*(s+s.^0.5./A)));
   end
   Ts(i,:)=sum(T);
end
end
```

## Appendix D Governing Equations for Heat Transport from HydroGeoSphere User Manual

$$[(\partial \rho_b c_b T)/\partial t] = -\nabla[\mathbf{q}\rho_w c_w T - (k_b + c_b \rho_b \mathbf{D})\nabla T] \pm Q_T + \Omega_o$$

$$D_{yy} = \alpha_{th}(q_x^2)/|q| + \alpha_l(q_y^2)/|q| + \alpha_{tv}(q_z^2)/|q| + D^*$$